GA-1508
Metallurgy and Ceramics
TID-4500 (15th ed.)

GENERAL DYNAMICS

MARITIME GAS-COOLED REACTOR PROGRAM

REACTOR MATERIALS COMPATIBILITY WITH IMPURITIES IN HELIUM

Work done by:

J. C. Bokros
H. E. Shoemaker

Report written by:

J. C. Bokros
H. E. Shoemaker

GENERAL ATOMIC DIVISION

Contract AT(04-3)-187 with the
U. S. Atomic Energy Commission
and the Maritime Administration

January 12, 1961

DISCLAIMER

CONTENTS

INTRODUCTION

The investigation of gas–metal interactions and the transport of carbon by trace impurities in helium was undertaken to determine the feasibility of graphite moderation for the Maritime Gas-cooled Reactor (MGCR).[1]* One of the proposed designs for this shipboard reactor utilized unclad graphite as the moderator and reflector, with helium as the coolant. Corrosion of reactor materials by the helium coolant would, of course, not be a problem; however, impurities that would evolve from graphite or that might find their way into the system in the make-up gas or through leaks could react with reactor materials at high temperatures and result in their deterioration.

The impurities which evolve from graphite during outgassing are predominantly carbon monoxide, hydrogen, nitrogen, and hydrocarbons. Impurities introduced either in the make-up gas or through leaks would probably be water vapor, oxygen, or nitrogen. The oxygen, when exposed to graphite in the reactor core in the temperature range 800° to 1700°F, would rapidly react with the graphite to form a mixture of carbon monoxide and carbon dioxide. The equilibrium ratio of carbon monoxide to carbon dioxide for a system containing graphite and a constant amount of oxygen has been plotted in Fig. 1. The parameter K_0 refers to the total partial pressure of oxygen compounds, if they were all converted to carbon monoxide, and is equal to the sum of the partial pressure of carbon monoxide and twice the partial pressure of carbon dioxide. For values of $(P_{CO} + 2P_{CO_2})$ that can be expected in the reactor system (less than 10^{-2} atm), the oxygen at equilibrium with graphite in the high-temperature regions of the core (above ~1200°F) will be present mainly as carbon monoxide. At lower temperatures the reaction

$$2CO \quad C + CO_2$$

*References are listed at the end of this report.

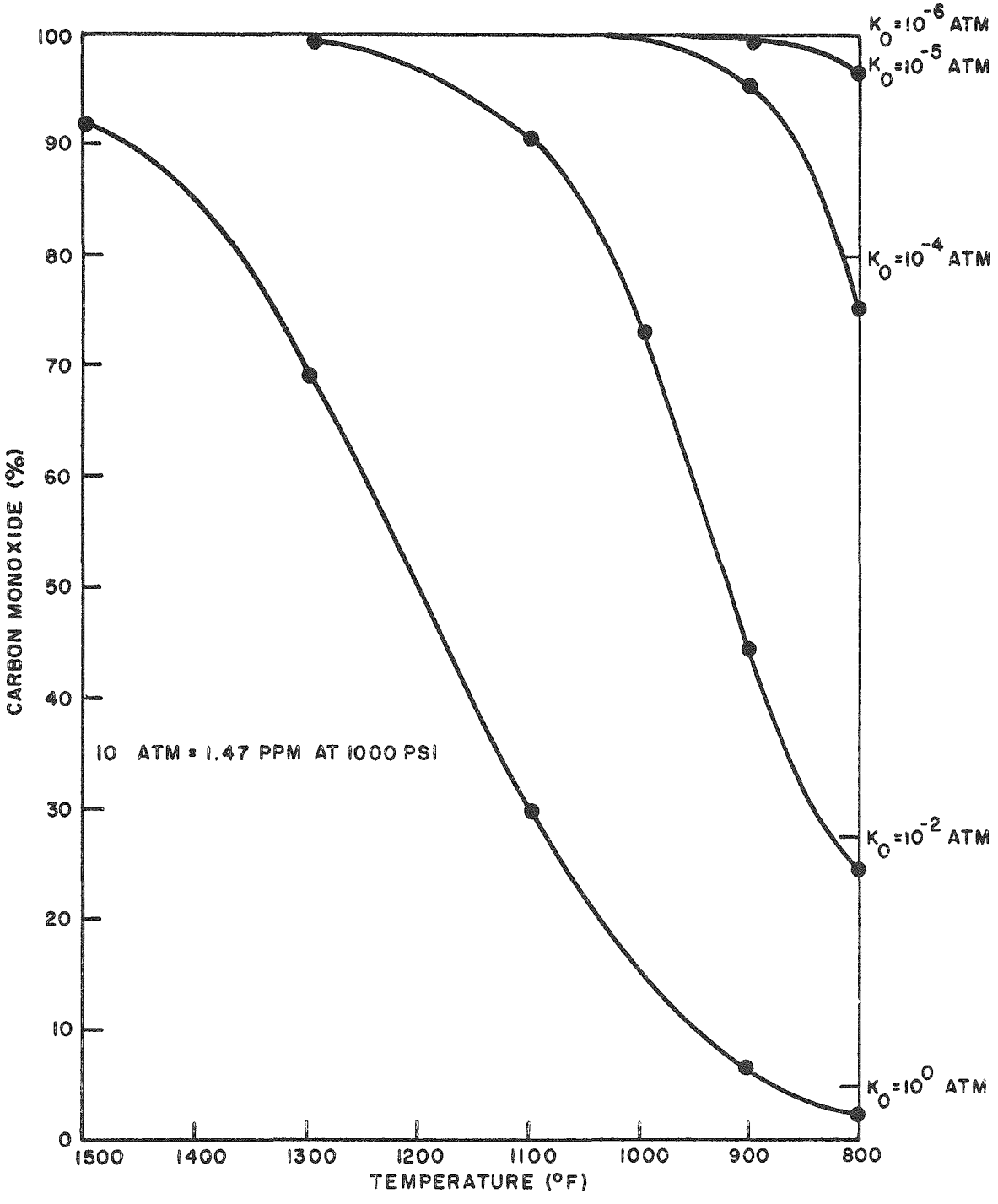

Fig. 1--Carbon monoxide—carbon dioxide equilibrium isograms for a constant oxygen content in equilibrium with graphite

tends to shift to the right, depositing carbon. This disproportionation is known to be catalyzed by many metallic surfaces.

Ragone[2] has considered the steps involved in the catalytic disproportionation of carbon monoxide on metallic surfaces and has calculated the rate of disproportionation in the MGCR system, assuming that the rate-limiting step involves the transport of carbon monoxide to the surface through a boundary layer and that an active metallic surface is available to catalyze the disproportionation. A complete literature survey of the catalytic disproportionation by metallic surfaces is also given by Ragone. Baukloh and Henke[3] have found that iron, nickel, and cobalt were strongly active catalysts, whereas silver, copper, zinc, silicon, molybdenum, tungsten, paladium, platinum, and the oxides of copper, silver, zinc, aluminum, titanium, silicon, vanadium, chromium, and manganese were intermediate in their catalytic activity. It is fairly well established that the active catalytic site is metallic and not a carbide. Catalytic surfaces of iron which had been deactivated by Fe_3C formation were found to be reactivated by a hydrogen treatment which removed the carbide.[4-8] These results point out the importance of selecting alloys for use in the reactor piping that either are inactive catalysts or form stable oxide films which poison the catalytic metallic surface in carbon monoxide.

The complex heat-resistant iron- and nickel-base alloys contain a large number of alloying elements; some can be oxidized by the ratio of CO/CO_2 in equilibrium with graphite, whereas others can be carburized by the ratio of CO/CO_2 in equilibrium with graphite, depending on the temperature of the graphite and the metal and on the total amount of oxygen in the system. The free energies of formation of the oxides and carbides of elements frequently found in heat-resistant alloys and carbon monoxide at various partial pressures are plotted in Fig. 2. At temperatures above about 1200°F and at carbon monoxide partial pressures below about 10^{-3} atm, iron and molybdenum form carbides, whereas zirconium and aluminum in the temperature range encountered in the MGCR (<1800°F) are

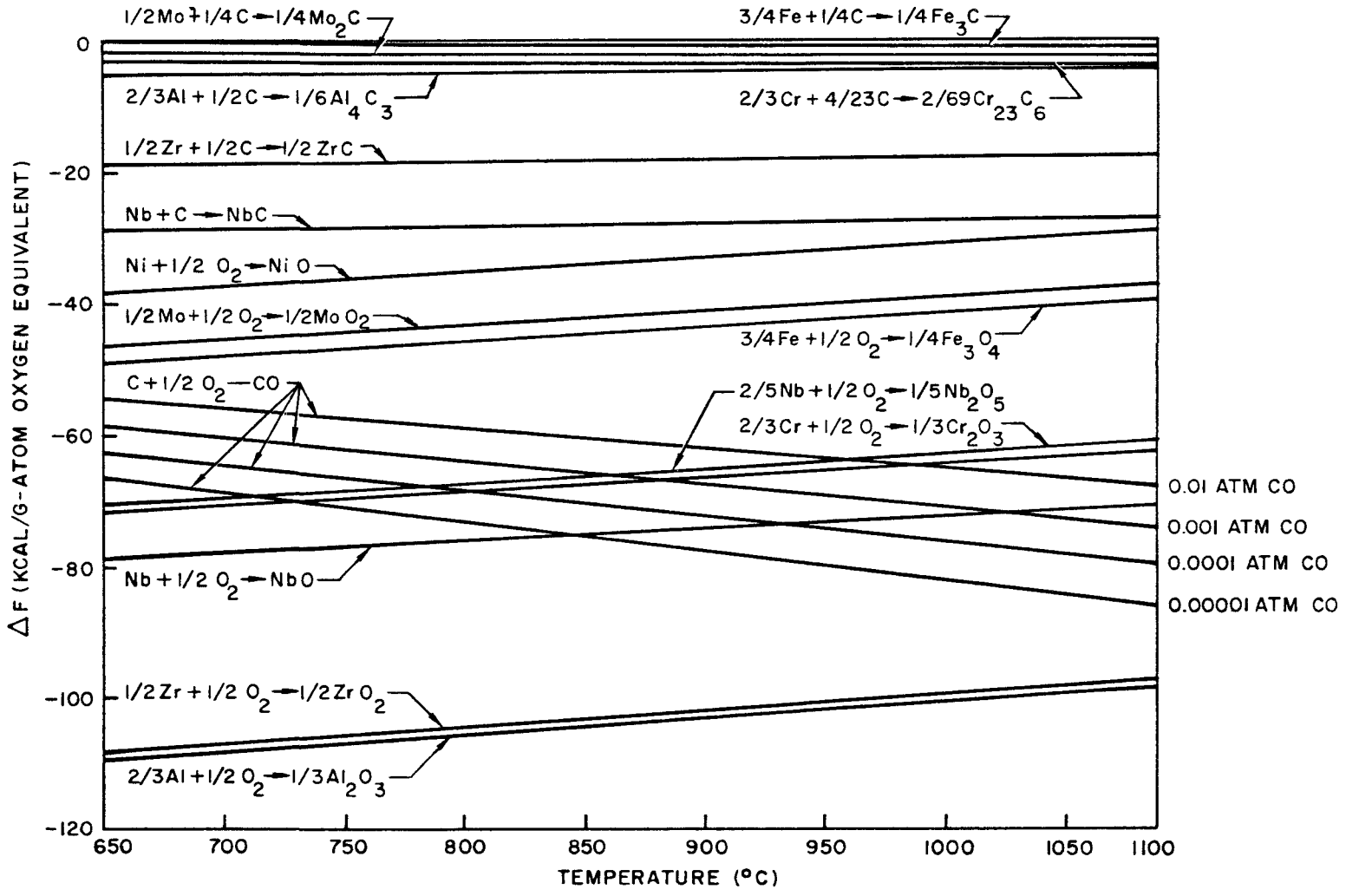

Fig. 2--Free energies of formation of the oxides and carbides of metals and of carbon monoxide at various partial pressures

oxidized. Chromium and niobium are elements which can be either oxidized or carburized in the temperature range of interest, depending on the partial pressure of carbon monoxide and the temperature. Whether or not a complex heat-resistant alloy is oxidized and/or carburized by the environments expected in the MGCR had to be determined experimentally.

The performance of niobium and its alloys in the environments described above is particularly important, since this class of alloys offers an attractively low-neutron-capture cross section for thermal reactors and very good high-temperature strength. Like chromium, these alloys can be oxidized and/or carburized by the CO-CO_2 mixtures expected in the MGCR. Unfortunately, because niobium and its alloys dissolve appreciable quantities of oxygen they are not protected by their oxides in temperature ranges where oxygen diffusion rates in the metal are high.

The purpose of this investigation was therefore fourfold: (1) to determine the maximum permissible partial pressure of carbon dioxide that could be tolerated in the reactor system without oxidizing and embrittling niobium and its alloys; (2) to screen the heat-resistant nickel- and iron-base alloys for resistance to oxidation and carburization by various partial pressures of H_2, CO, and CO_2; (3) to rank the heat-resistant alloys according to their catalytic influence on the disproportionation of carbon monoxide; and (4) to study the effect of hydrogen additions on the carburization of the heat-resistant alloys and on the decomposition of carbon monoxide.

MATERIALS

The graphite specimens used in these tests were all machined from AGOT graphite blocks. The metals selected for evaluation were those of interest to the MGCR for such applications as fuel cladding, turbine blades, pressure vessels, piping, etc. These metals included niobium and niobium alloys, nickel and nickel alloys, austenitic and ferritic stainless steels, low-alloy steels, and molybdenum (see Table 1).

Table 1

ANALYSIS OF MATERIALS SELECTED FOR TESTING

Alloy Type	Designation	Composition (%)									
		C	Mn	P	S	Si	Ni	Cr	Mo	Nb	Other
Austenitic stainless steel	316	0.08	1.51	0.02	0.02	0.51	10.98	17.43	2.43	----	
Ferritic alloys	430	0.05	0.46	0.014	0.010	0.33	-----	15.56	----	----	
	9 Cr–1 Mo	0.12	0.37	0.010	0.009	0.30	-----	8.60	1.07	----	
	5 Cr–1/2 Mo	0.11	0.37	0.012	0.011	0.41	-----	4.60	0.53	----	
	2-1/4 Cr–1 Mo	0.10	0.44	0.019	0.012	0.26	-----	2.26	0.98	----	
	1-1/4 Cr–1/2 Mo	0.12	0.45	0.012	0.023	0.65	-----	1.20	0.52	----	
	Croloy	----	----	-----	-----	----	-----	0.25	----	----	
	C–Mo	0.12	0.42	0.014	0.016	0.21	-----	-----	0.54	----	
Nickel-base alloys	"A" Nickel	0.10	----	-----	-----	----	99.4	-----	----	----	Cu, 0.10; Fe, 0.15 (nominal)
	Monel	0.15	1.00	-----	0.01	0.1	67	-----	----	----	Fe, 1.4; Cu, 30
	Inconel	0.04	0.21	-----	0.007	0.19	76.80	15.46	----	----	Cu, 0.06; Fe, 6.76
	Inconel X	0.05	0.56	-----	0.007	0.31	72.77	15.32	----	1.01	Cu, 0.08; Al, 0.71; Ti, 2.47; Fe, 6.69
	Inconel 702	0.04	0.1	-----	-----	0.25	79	15.5	----	----	Fe, 0.50; Al, 3
Refractory metals	Molybdenum	----	----	-----	-----	----	-----	-----	100	----	
	Niobium	----	----	-----	-----	----	-----	-----	----	100	
	Nb–1 Zr	----	----	-----	-----	----	-----	-----	----	99	
	Nb–5 Zr	----	----	-----	-----	----	-----	-----	----	95	
	Nb–5 Ti	----	----	-----	-----	----	-----	-----	----	95	
	Nb–8 Ti	----	----	-----	-----	----	-----	-----	----	92	
	Nb–10 Ti	----	----	-----	-----	----	-----	-----	----	90	
	Nb–20 Ti	----	----	-----	-----	----	-----	-----	----	80	
	Copper	----	----	-----	-----	----	-----	-----	----	----	

The helium used was Bureau of Mines grade A helium. An average analysis for the gas as received was H_2, 0. 1 ppm; Ne, 15 ppm; N_2, 1 ppm; O_2, 0. 5 ppm; and H_2O, 10 ppm. This gas was further purified by passing it through a 5A molecular sieve, a titanium-chip trap at 1500°F, and a uranium-chip trap at 1000°F. This treatment reduced H_2O to less than 5 ppm and maintained O_2 at less than 1 ppm.

The carbon dioxide used as a contaminant was Liquid Carbonic's welding grade, 99. 9% pure. The carbon monoxide used was Matheson's high-purity grade, which contained 99. 8% CO and 0. 2% N_2, and it was passed through a 5A molecular sieve to remove traces of CO_2 and H_2O. The impurity level was reduced to 3. 5 ppm H_2O with no detectable CO_2. The hydrogen used was Liquid Carbonic's pure grade, which was further purified by passing it through a 5A molecular sieve to remove moisture. There were no detectable impurities shown by gas chromatographic methods. The methane was Matheson's commercial grade, which contained 94. 16% methane, 0. 48% carbon dioxide, 0. 23% nitrogen, 3. 24% ethane, 1. 12% propane, 0. 23% isobutane, 0. 23% n-butane, 0. 13% isopentane, 0. 08% n-pentane, 0. 07% heptane, and higher hydrocarbons. It was further purified by passing it through a 5A molecular sieve to remove all detectable carbon dioxide.

APPARATUS AND EXPERIMENTAL PROCEDURE

The apparatus constructed for this investigation is shown schematically in Fig. 3. In this system, trace impurities or mixtures of impurities were introduced into the purified helium stream through a controlled variable leak. The helium containing controlled amounts of impurities was passed over the test specimens, which were suspended on alumina racks in fused silica reaction chambers. The apparatus was constructed so that gas samples could be bypassed through a gas chromatograph from both the inlet and the exhaust of each reaction chamber. The flow rate was measured by

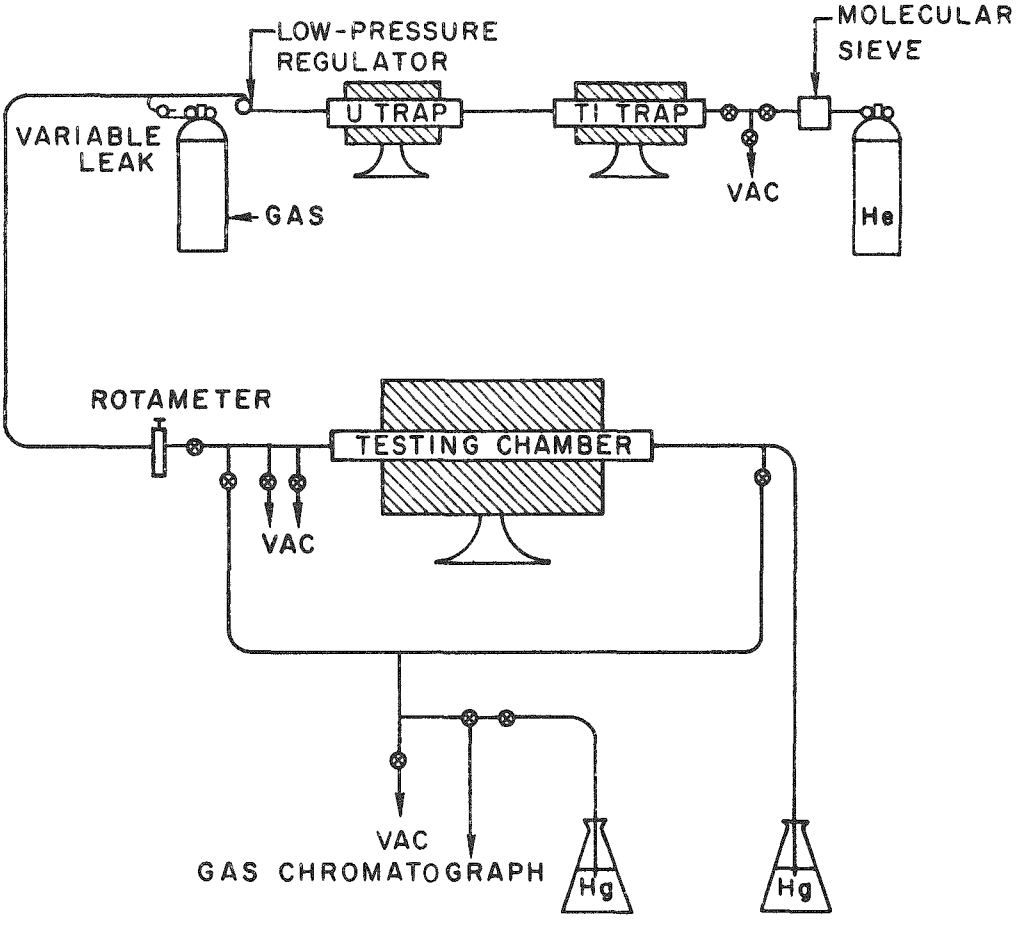

Fig. 3--Schematic diagram of apparatus for testing helium impurity reactions with graphite and metal

passing the gas stream through a rotameter at 1/4 ft^3/hr, which corresponds to a linear flow of 4 in./min over the test specimens. The gas was exhausted through a mercury trap to prevent back diffusion of atmospheric gases and to maintain a slight positive pressure in the system.

Each reaction chamber was surrounded by a resistance furnace with separate temperature controls for the front and rear sections. With this arrangement it was possible to maintain either a constant temperature or a controlled temperature gradient in each test chamber. The specimen temperatures were measured with thermocouples introduced from both ends of the chambers.

A test was conducted by inserting the weighed graphite and/or metal specimens, evacuating the system, and heating to the test temperature slowly enough to maintain the system pressure below 1 μ Hg. After the test temperature had been reached, pure helium was flushed through the system to remove the remaining impurities, and the test gas (helium plus controlled impurities) was admitted to the test chamber. The inlet and outlet gas was periodically analyzed to maintain the correct gas composition. Periodically, the furnaces were cooled and the specimens removed for examination; each specimen was weighed and photographed immediately after removal from the test chamber. X-ray diffraction patterns were obtained from the surface of selected test pieces to determine the identity of the corrosion products. The specimens were then nickel-plated, sectioned, and prepared for metallographic examination. The depth of penetration was measured and the microstructural changes were recorded. Microhardness measurements were obtained on each sample at the center and the edge. Sections of each specimen were analyzed for carbon and oxygen for comparison with analyses of corresponding untested samples.

CHEMICAL ANALYSES

The analysis of gas samples was conducted with a Loenco Model 11 Chromat-O-Flex gas chromatograph. The detector unit contained four

hot-wire-filament thermal-conductivity cells. The gas for analysis was conducted through copper tubing to the chromatograph. Samples taken from the gas stream for analysis were passed through a 6-ft, 5A molecular sieve column for the separation and determination of H_2, O_2, N_2, CH_4, and CO. A 6-ft silica gel column was used for the analysis of CO_2. This method of analysis, using a 3-ml sample, was accurate to ±5 ppm for all gases except H_2. For the analysis of a constituent of a lower concentration than 5 ppm, it was necessary to use a concentrated sample. A 1-liter gas sample was concentrated by passing the gas through an activated charcoal trap submerged in liquid nitrogen, which left the impurities adsorbed on the charcoal. The liquid nitrogen was removed and the sample injected into the chromatograph for analysis. By using this method of sampling, the sensitivity of the analysis was increased over 300 times; however, there was a loss in accuracy due to the imperfect concentration. Average analyses of the gases are listed in Table 2.

The analysis for carbon in the metal specimens was conducted in two ways. A gravimetric method of analysis was used for samples thought to contain more than 0.05% carbon. This method was accurate for a 1-g sample in the range from 0.1% to 100% carbon. For this analysis, the metal specimen was oxidized at 1100° to 1200°C in a stream of purified oxygen, and the carbon dioxide that formed was trapped from the gas stream as it passed through a weighed Ascarite trap. The weight gained by the Ascarite was an indication of the carbon in the sample. A conductimetric analysis was used for samples thought to contain less than 0.05% carbon. For a 1-g sample, this method was accurate in the range from 0.035% to 0.001% carbon. For this type of analysis, the metal specimen was burned in an induction furnace while purified oxygen was passed through the system. The carbon dioxide thus produced from the carbon in the specimen was passed into a barium hydroxide solution, and the carbon content was determined from the change in resistivity of the solution.

Table 2

AVERAGE STEADY-STATE GAS ANALYSES

Material Tested	Gas Sample Location	Concentrations of Gases							Remarks
		H_2 (%)	O_2 (ppm)	N_2 (ppm)	CO (%)	CH_4 (%)	CO_2 (%)	H_2O (%)	
Ni, Ni-base alloys, steels:									
In 0.5 atm CO + 0.5 atm H_2	Inlet	50	70	700	50	---	0.07	15-40	
flowing at 3/4 ft^3/hr	Outlet	48	5	750	48	1	2	1	
In 5×10^{-3} atm CO + 5×10^{-3}	Inlet	0.5	----	10-20	0.5	---	----	10-40	
atm H_2 flowing at 1/4 ft^3/hr	Outlet	0.5	----	10-20	0.5	+	<10	10-40	
Molybdenum:									
In 5×10^{-3} atm CO + 5×10^{-3}	Inlet	0.5	4-5	20	0.5	---	----	40	
atm H_2 flowing at 1/4 ft^3/hr	Outlet	0.5	----	20	0.5	0.4	<10	40	
Nb and Nb alloys:									
In 5×10^{-3} atm CO + 5×10^{-3}	Inlet	0.5	----	20	0.5	---	----	6-20	
atm H_2 flowing at 1/4 ft^3/hr	Outlet	0.5	----	20	0.5	---	<10	6-20	
Carbon:									
In 0.5 atm CO + 0.5 atm H_2	Inlet	60	----	0.04	40	---	----	(*)	
flowing at 3/4 ft^3/hr	Outlet	60	----	0.04	40	0.7	0.8	(*)	
In 1 atm H_2 flowing at	Inlet	100	(*)	20-40	---	---	----	(*)	
1.5 ft^3/hr	Outlet	100	(*)	20	30	240	----	(*)	
In 1 atm CH_4 flowing at	Inlet	---	0.46	0.7	---	96	----	(*)	3.8% heavy hydrocarbons
1.5 ft^3/hr	Outlet	+	0.04	0.7	---	86	----	(*)	Complex, 70% aromatic

*No analysis for this component.

Exposure in 2×10^{-4} atm ($P_{CO} + 2P_{CO_2}$)

For the tests conducted in helium plus 2×10^{-4} atm ($P_{CO} + 2P_{CO_2}$), perforated graphite plugs were placed at each end of the furnace in a quartz reaction chamber. The specimens, graphite disks and metal pieces, were alternately spaced on an alumina rod, using alumina spacers to prevent contact with adjacent specimens, and were placed in a graphite tube as shown Fig. 4. The tube was inserted in the reaction chamber so that it rested in the constant-temperature zone at the center of the furnace.

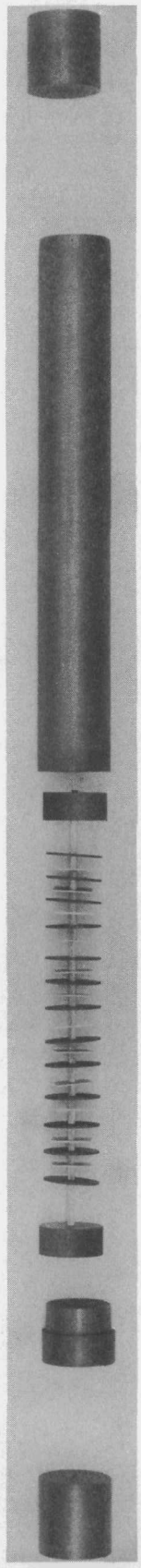

Fig. 4--Experimental test loading

Two reaction tubes were loaded with samples of niobium and niobium + 1% Zr and two tubes were loaded with graphite, "A" nickel, Inconel X, Inconel, Monel, Type 430 stainless steel, and Type 316 stainless steel. One tube of each group of materials was exposed at 1700°F and the other tubes were exposed at 1500°F.

The impurity level was monitored at all times at the inlet and exhaust of the reaction tubes. When the impurities were outgassed from the system, the trace impurity (80 ppm of CO_2) was added to the helium stream through a controlled leak. On entering the reaction chamber, the gas passed through the front perforated graphite plug, whose temperature was maintained at about 1200°F; the

carbon dioxide was partially converted to carbon monoxide at this point. This gas then passed through the perforated graphite plugs (shown in Fig. 4) and over the metal and graphite samples. After leaving the graphite cylinder, the gas passed through another graphite plug at the exhaust. The temperature of the exhaust porous-graphite plug was 1100° to 1200°F on the inside face and 800° to 900°F on the outside face. The exhaust gas required about 4 sec to pass through the graphite end plug, after which it cooled to room temperature in about 1 min. This quench was apparently rapid enough to prevent the disproportionation of carbon monoxide in the absence of an appropriate catalyst, as indicated by the absence of weight gain in the exhaust plugs and the presence of less than 1 ppm CO_2 in the exhaust gas.

Niobium and niobium + 1% Zr were oxidized and carburized when exposed to 2×10^{-4} atm CO + CO_2. At 1700°F, the average carbon concentration in niobium increased from 0.005% to about 0.040% in 500 hr; at 1500°F the carbon content increased by a factor of 2 to 3 in 500 hr (see Table 3). The carburization occurred as a thin layer of NbC and Nb_2C, 0.1 to 0.3 mils thick, which, after it had formed, grew slowly in thickness. In addition to the carburization, the two niobium specimens exposed in positions 1 and 2* at 1500°F became very brittle in 400 to 500 hr. X-ray diffraction patterns taken from the surface of the embrittled specimens revealed the two oxides NbO and NbO_2. Metallographic examination showed pits 6 to 8 mils deep that contained a white and a gray phase, presumably NbO and NbO_2 (see Fig. 5). Macroscopically, these pits appeared as surface blisters.

The results for the niobium + 1% Zr alloy were similar to those for niobium. The two carbides NbC and Nb_2C were found on specimens at 1500° and 1700°F. The specimens in position 1 at 1500°F became very

*The graphite specimen chamber was divided into four positions of equal length which were numbered from 1 to 4 going from the inlet to the outlet.

Table 3

SUMMARY OF RESULTS FOR METALS EXPOSED TO 2×10^{-4} ATM ($P_{CO} + 2P_{CO_2}$)

Material	Time (hr)	Temp. (°F)	Zone	Penetr. (mils)	Per cent Carbon		Corrosion Products*	Remarks
					Initial	Final		
Niobium (C.P.)	94	1500	1	0.1	0.005	0.005	$(Nb_2C)_m$, $(NbC)_w$	Carbide surface layer
	406	1500	1	8.0	0.005	0.01	$(Nb_2C)_s$, $(NbC)_s$, $(NbO)_w$, $(NbO_2)_w$	Oxide pits; brittle
	500	1500	4	0.2	0.005	0.14	$(Nb_2C)_s$, $(NbC)_s$	Carbide surface layer
	94	1700	1	0.2	0.005	0.25	$(NbC)_s$, $(Nb_2C)_s$	Carbide surface layer
	406	1700	1	0.1	0.005	0.27	$(NbC)_s$, $(Nb_2C)_s$	Carbide surface layer
	500	1700	4	0.1	0.005	0.35	$(NbC)_s$, $(Nb_2C)_s$	Carbide surface layer
Niobium + 1% Zr	94	1500	1	0.3	0.004	0.007	$(Nb_2C)_m$, $(NbC)_w$	Carbide surface layer
	406	1500	1	0.1	0.004	0.004	$(Nb_2C)_s$, $(NbC)_m$	Carbide surface layer; brittle
	500	1500	4	0.1	0.004	0.015	$(Nb_2C)_s$, $(NbC)_m$	Carbide surface layer
	94	1700	1	0.1	0.004	0.24	$(Nb_2C)_m$, $(NbC)_m$	Carbide surface layer
	406	1700	1	0.5	0.004	0.46	$(Nb_2C)_s$, $(NbC)_s$	Carbide surface layer
	500	1700	4	0.3	0.004	0.41	$(Nb_2C)_s$, $(NbC)_s$	Carbide surface layer
Type 430 SS	406	1500	1	<0.1	0.078	0.066	$(Spinel)_s$	
	500	1500	4	<0.1	0.078	0.071	$(Spinel)_m$	
	406	1700	4	0.5	0.078	0.141	$(Spinel)_s$, $(Cr_2O_3)_w$	Carburized
	500	1700	1	0.8	0.078	0.152	$(Spinel)_s$, $(Cr_2O_3)_w$	Carburized

*The subscript s is the small diffraction pattern; m, the medium diffraction pattern; and w, the weak diffraction pattern.

Table 3--continued

Material	Time (hr)	Temp. (°F)	Zone	Penetr. (mils)	Per cent Carbon		Corrosion Products*	Remarks
					Initial	Final		
Type 316 SS	406	1500	1	0.2	0.066	0.072	$(Spinel)_s$	
	500	1500	4	0.1	0.066	0.070	$(Spinel)_m$	
	406	1700	4	0.2	0.066	0.098	$(Spinel)_s, (Cr_2O_3)_w$	
	500	1700	1	0.2	0.066	0.120	$(Spinel)_s, (Cr_2O_3)_w$	
Inconel	406	1500	1	0.4	0.004	0.001	$(Cr_2O_3)_s, (Spinel)_w$	
	500	1500	4	0.5	0.004	0.004	$(Cr_2O_3)_w, (Spinel)_w$	
	406	1700	4	0.2	0.004	0.001	$(Cr_2O_3)_w$	
	500	1700	1	0.3	0.004	0.008	$(Cr_2O_3)_w$	
Inconel X	406	1500	1	0.7	0.032	0.010	$(Cr_2O_3)_s, (Spinel)_m$	
	500	1500	4	0.6	0.032	0.024	$(Cr_2O_3)_w$	
	406	1700	4	0.2	0.032	0.016	$(Cr_2O_3)_w$, (Spinel)	
	500	1700	1	0.2	0.032	0.033	$(Cr_2O_3)_w, (Spinel)_w$	
"A" Nickel	100	1500	1	<0.1	0.065	0.001	None	
	500	1500	4	<0.1	0.065	0.034	None	
	100	1700	4	<0.1	0.065	0.076	None	
	500	1700	1	<0.1	0.065	0.061	None	

*The subscript s is the small diffraction pattern; m, the medium diffraction pattern; and w, the weak diffraction pattern.

Table 3--continued

Material	Time (hr)	Temp. (°F)	Zone	Penetr. (mils)	Per cent Carbon		Corrosion Products	Remarks
					Initial	Final		
Monel	406	1500	1	2.0	0.071	0.001	None	Intergranular attack
	406	1500	4	<0.1	0.071	0.043	None	
	406	1700	1	<0.1	0.071	0.049	None	
	406	1700	4	<0.1	0.071	0.074	None	
Duranickel	406	1500	1	0.5	0.132	0.132		
	406	1500	4	<0.1	0.132	0.111		

Fig. 5--Photomicrograph of niobium exposed for 500 hr at 1500°F in helium + 2×10^{-4} atm ($P_{CO} + 2P_{CO_2}$)--large pit 6.0 mils deep; corrosion products: NbC, Nb_2C, NbO, NbO_2 (500×)

brittle in 500 hr and the hardness data indicated that oxygen contamination had occurred at 1500° and 1700°F. Typical weight gain versus time data (Figs. 6 and 7) show relatively small weight gains, with the largest changes occurring on samples exposed in position 1--the more oxidizing position. The metallographic and diffraction data are summarized in Table 3.

Types 430 and 316 stainless steel showed little evidence of carburization after 500 hr at 1500°F in 2×10^{-4} atm ($P_{CO} + 2P_{CO_2}$); however, when exposed at 1700°F, chemical analysis revealed that both alloys increased significantly in carbon content. The microstructure of Type 430 stainless steel carburized at 1700°F is shown in Fig. 8. Both of these stainless steels were oxidized by this environment at 1500° and 1700°F and formed surface films of spinel and Cr_2O_3. The maximum oxide penetration in all cases was less than 1.0 mil (see Figs. 9a and b).

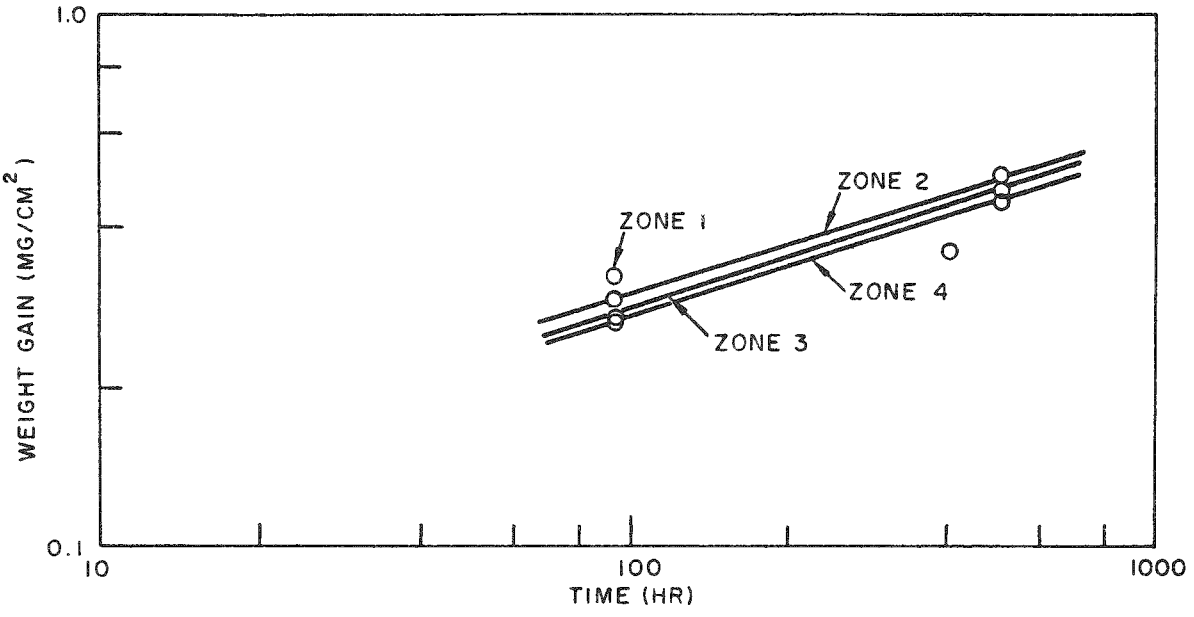

Fig. 6--Weight gain versus time for niobium in helium + 2×10^{-4} atm ($P_{CO} + 2P_{CO_2}$) at 1700°F

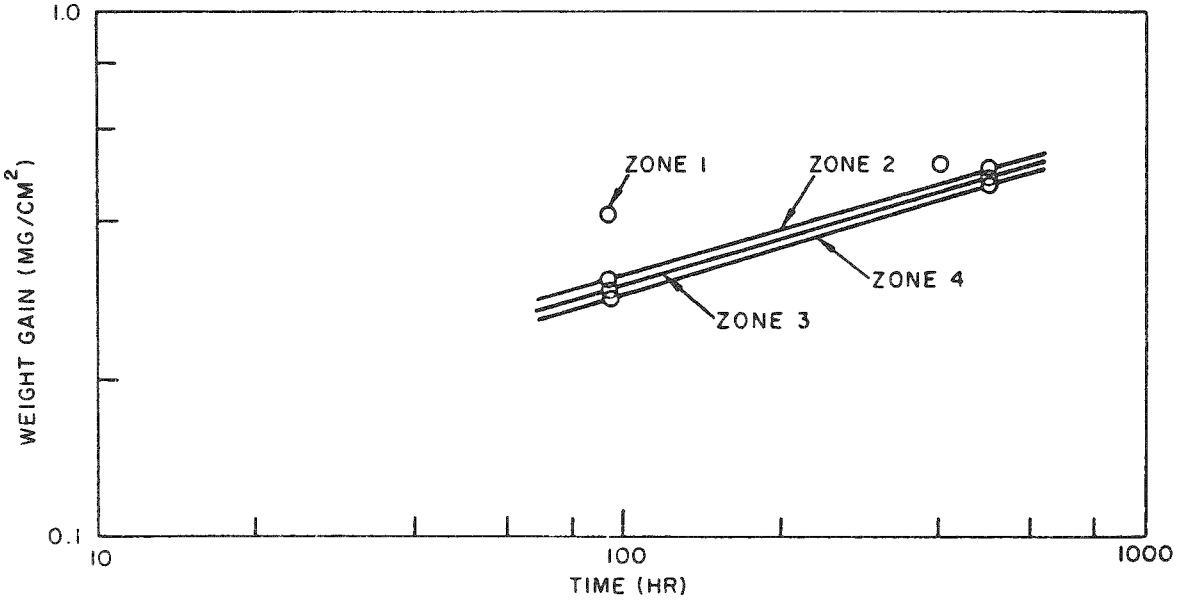

Fig. 7--Weight gain versus time for niobium + 1% Zr in helium + 2×10^{-4} atm ($P_{CO} + 2P_{CO_2}$) at 1700°F

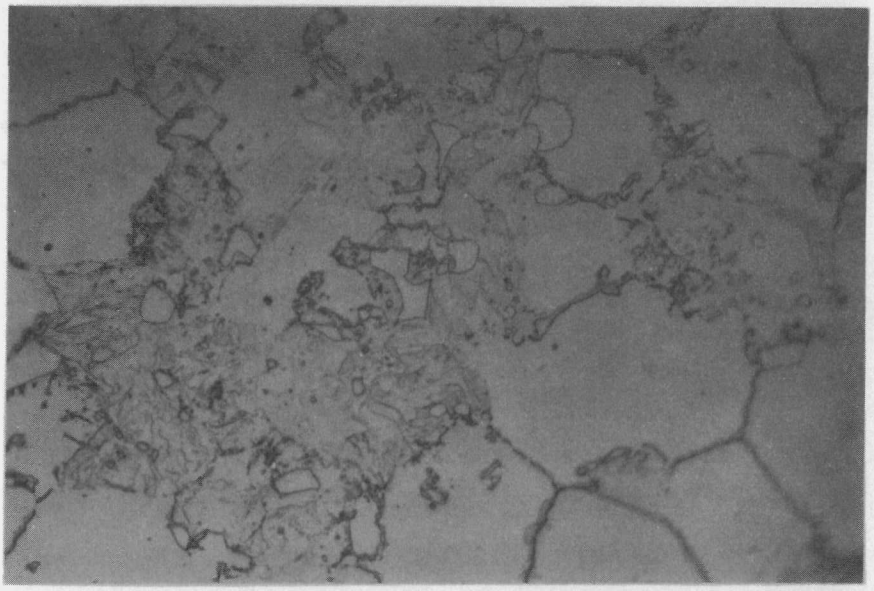

Fig. 8--Microstructure of Type 430 stainless steel exposed for 500 hr at 1700°F in helium + 2×10^{-4} atm ($P_{CO} + 2P_{CO_2}$)--completely carburized (500×)

Chemical analysis of Inconel and Inconel X specimens exposed in 2×10^{-4} atm ($P_{CO} + 2P_{CO_2}$) indicated that little, if any, carburization occurred at either 1500° or 1700°F. These results were substantiated by metallographic examination. The corrosion products identified on the surface of these alloys after exposure were mainly Cr_2O_3 and spinel and in all cases were less than 1 mil thick.

"A" nickel formed no surface reaction products in this atmosphere. It decarburized in all positions at 1500°F and decarburized in positions 1, 2, and 3 in 500 hr at 1700°F. Metallographic examination revealed no significant attack.

The behavior of Monel was similar to that observed for nickel. All specimens decarburized at 1500°F and the specimens in positions 1, 2, and 3 decarburized at 1700°F. The specimens in position 4 at 1700°F carburized slightly. Metallographic examination revealed an intergranular attack to a maximum depth of 2 mils on samples exposed in positions

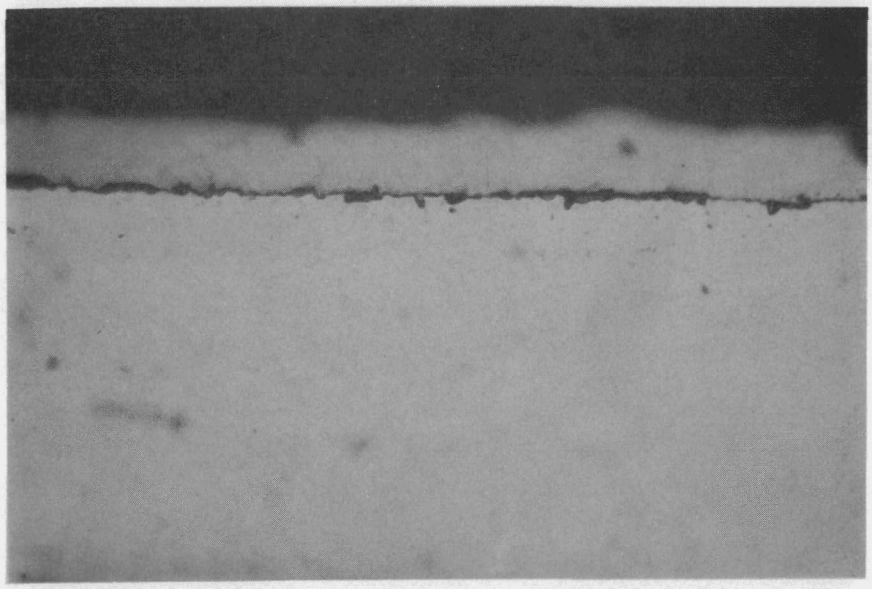

(a) Type 316 stainless steel

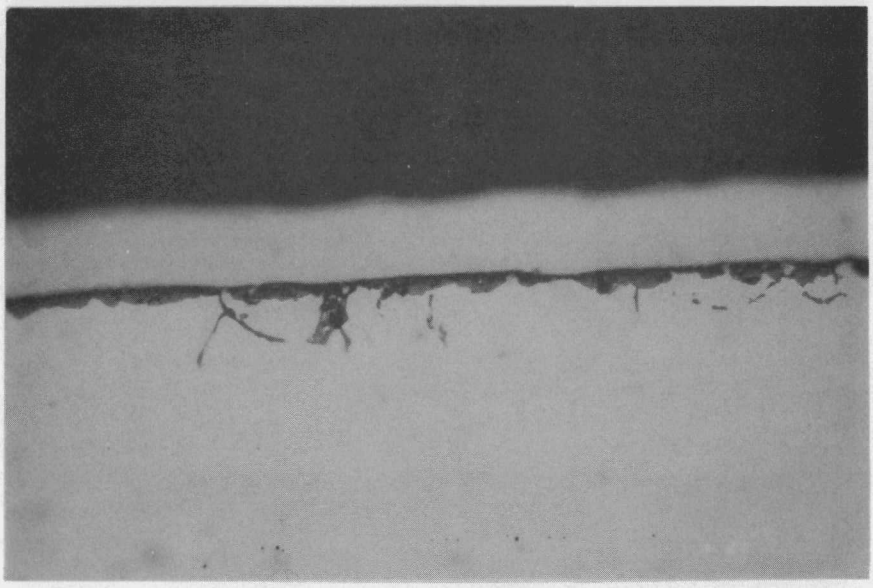

(b) Type 430 stainless steel

Fig. 9--Surface oxide formed on stainless steel exposed for 500 hr at 1700°F in helium + 2×10^{-4} atm ($P_{CO} + 2P_{CO_2}$)--corrosion products: spinel and $(Cr, Fe)_2O_3$ (500×)

1 and 2 for 406 hr at 1500°F (see Fig. 10). This was probably due to alternate oxidizing and reducing conditions at the inlet end of the graphite tube.

No carbon transport was observed at the partial pressure 2×10^{-4} atm ($P_{CO} + 2P_{CO_2}$).

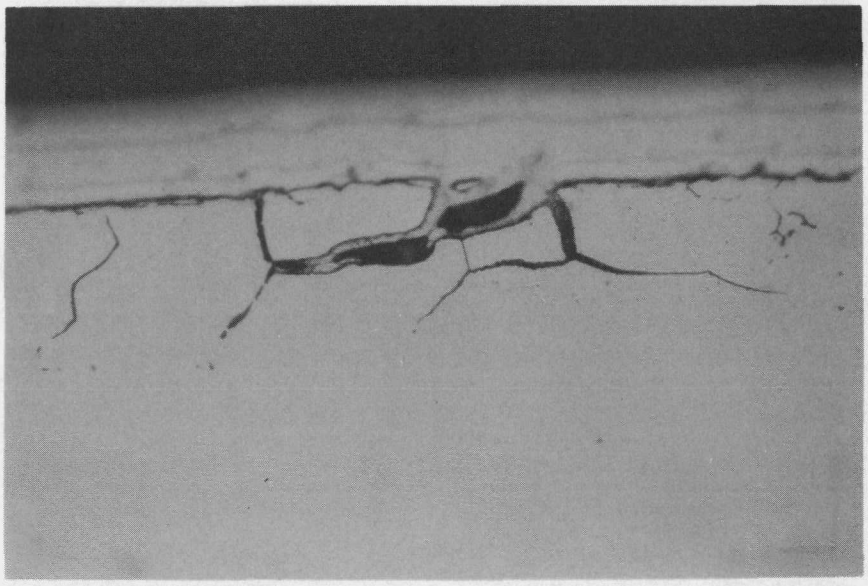

Fig. 10--Photomicrograph of Monel exposed for 406 hr at 1500°F in helium + 2×10^{-4} atm ($P_{CO} + 2P_{CO_2}$)-- intergranular attack 1.5 mils deep (500×)

Exposure in 10^{-2} atm ($P_{CO} + 2P_{CO_2}$)

The 10^{-2} atm ($P_{CO} + 2P_{CO_2}$) tests were conducted in a manner very similar to the 2×10^{-4} atm ($P_{CO} + 2P_{CO_2}$) tests, except that graphite and metal specimens were placed alternately in the exhaust end of the furnace to study the reactions of the gases on the metals at lower temperatures. The metallographic and diffraction data are summarized in Table 4.

During the first 100 hr of this exposure, carbon dioxide was metered into the helium stream, reacted with graphite at 1700°F, and passed over the specimen, also at 1700°F. During the following 400 hr of exposure,

Table 4

SUMMARY OF RESULTS FOR METALS EXPOSED TO 10^{-2} ATM ($P_{CO} + 2P_{CO_2}$)

Material	Time (hr)	Temp. (°F)	Zone*	Penetr. (mils)	Per cent Carbon		Corrosion Products†	Weight Change (mg/cm^2)	Remarks
					Initial	Final			
Niobium	500	1700	3	18.0	0.001	2.40	$(NbC)_s, (NbO_2)_m$	+23.0	Oxide-carbide surface layer
	500	1700	2	14.0	0.001	1.90	$(NbC)_s, (NbO_2)_m$	+25.0	Oxide-carbide surface layer
	100	1700	1	6.0	0.001	-----	$(NbC)_m, (NbO)_m, (NbO_2)_s, (NbO_2O_5)_w$	+5.25	Pits
Niobium + 1% Zr	100	1700	1	12.0	0.004	-----	$(NbC)_s, (NbO)_s, (NbO_2)_s, (Nb_2O_5)_m$	+10.06	
	500	1700	2	>30	0.004	1.21	$(NbC)_s, (NbO)_w, (NbO_2)_s$	+21.0	Grain-boundary attack
	500	1700	3	>30	0.004	1.29	$(NbC)_s, (NbO_2)_m$	+17.0	Grain-boundary attack
Niobium + 5% Zr	100	1700	1	3.0	0.020	-----	$(NbC)_s, (Nb_2C)_s, (NbO)_m, (NbO_2)_s$	+8.8	Pits
	500	1700	2	3.0	0.020	0.24	$(NbC)_s, (Nb_2C)_m, (NbO_2)_w$	+9.5	Oxide-carbide surface layer
	500	1700	3	15	0.020	0.23	$(NbC)_s, (Nb_2C)_w$	+8.7	Pits
Niobium + 5% Ti	400	1700	1	10.0	0.015	0.107	$(NbC)_s, (Nb_2C)_m, (TiC)_m$	+2.45	Solid-solution surface layer
	400	1700	2	6.0	0.015	0.137	$(NbC)_s, (Nb_2C)_w$	+1.32	Solid-solution surface layer
Niobium + 8% Ti	400	1700	1	0.1	0.030	0.28	$(NbC)_s, (Nb_2C)_w, (TiC)_w$	+1.42	
	400	1700	3	0.1	0.030	0.34	$(NbC)_s, (Nb_2C)_m, (TiC)_m$	+1.28	
Niobium + 10% Ti	400	1700	1	4.0	0.022	0.20	$(NbC)_s, (Nb_2C)_w, (TiC)_w$	+2.17	Solid-solution surface layer
	400	1700	2	5.0	0.022	0.23	$(NbC)_s, (Nb_2C)_w$	+1.75	Solid-solution surface layer
430 SS	500	1700	3	>30	0.08	0.122	$(Spinel)_s, (Cr_2O_3)_w$	+0.415	Completely carburized
	500	1700	1	>30	0.08	0.08	$(Spinel)_s, (Cr_2O_3)_w$	+0.265	Completely carburized
316 SS	500	840	4	<0.1	0.045	0.077	$(Spinel)_w, [(Cr, Fe)_2O_3]_s$	+0.07	
	500	1400	4	0.8	0.045	0.104	$(Spinel)_m, (Cr_2O_3)_w$	+0.73	Internal oxidation
	500	1700	3	0.8	0.045	0.121	$(Spinel)_s$	+0.25	Internal oxidation--scaling
Inconel	500	1700	1	1.2	0.016	0.030	$(Spinel)_m, [(Cr, Fe)_2O_3]_m$	+0.415	Internal oxidation
	500	1700	3	1.0	0.016	0.026	$(Spinel)_m, [(Cr, Fe)_2O_3]_m$	+0.435	Internal oxidation

*Zones 1 and 2 are at the inlet and zones 3 and 4 are at the outlet.

†The subscript s is the small diffraction pattern; m, the medium diffraction pattern; and w, the weak diffraction pattern.

Table 4--continued

Material	Time (hr)	Temp. (°F)	Zone*	Penetr. (mils)	Per cent Carbon		Corrosion Products†	Weight Change (mg/cm^2)	Remarks
					Initial	Final			
Inconel X	500	1700	1	1.8	0.035	0.067	$(Spinel)_s, [(Cr, Fe)_2O_3]_m$	+1.30	Internal oxidation
	500	1700	3	1.5	0.035	0.075	$(Spinel)_s, [(Cr, Fe)_2O_3]_m$	+1.22	Internal oxidation
	500	1300	4	6.0	0.035	0.22	None	+1.09	Carburized; 1.5-mil internal oxidation
"A" Nickel	500	1700	1	<0.1	0.011	0.008	None	-0.03	
	500	1700	3	<0.1	0.011	0.039	None	-0.66	
	500	1250	4	<0.1	0.011	0.074	None	-0.01	
Monel	500	1700	1	3.0	0.096	0.028	None	+0.13	Fine grain-boundary precipitate
	500	1700	3	7.0	0.096	0.035	None	+0.15	Fine grain-boundary precipitate
	500	1470	4	<0.1	0.096	0.049	None	+0.01	
	500	1140	4	<0.1	0.096	0.096	None	+0.09	

*Zones 1 and 2 are at the inlet and zones 3 and 4 are at the outlet.

†The subscript s is the small diffraction pattern; m, the medium diffraction pattern; and w, the weak diffraction pattern.

carbon monoxide instead of carbon dioxide was metered into the helium, reacted with graphite at 1700°F, and passed over the metal specimens. New alloy specimens were added after the first 100 hr and were exposed only to the helium + 10^{-2} atm CO.

The niobium-zirconium alloys tested for 100 hr were badly oxidized and carburized by this CO-CO_2 mixture and were completely embrittled. The weight gains of niobium-zirconium compared with pure niobium were large (see Figs. 11 and 12). Diffraction patterns taken from the surfaces of these specimens revealed the presence of the three oxides of niobium and the two carbides (see Table 4). Specimens present during both exposures formed surface oxides in the first 100 hr, which were reduced by the carbon monoxide in the last 400 hr. This was evidenced by the X-ray data obtained from specimens after 100 hr and again after 500 hr. Very strong oxide lines were obtained after the first 100-hr exposure in CO-CO_2 and disappeared or became much weaker in the subsequent 400-hr exposure to carbon monoxide. Specimens present only during the 400-hr period when carbon monoxide was metered into the helium stream formed surface layers containing only the carbides.

Metallographic examination revealed that the oxide-carbide layer penetrated to a depth of 6 to 12 mils in 100 hr at 1700°F. Figure 13 is a typical photomicrograph of this attack on niobium + 1% Zr.

The two stainless steels, Types 430 and 316, exposed at 1700°F, and the specimen of Type 316 exposed in the exhaust end of the tube at 1400°F, were carburized after the 500-hr exposure. Chemical analysis of the specimens before and after exposure revealed appreciable increases in carbon content, and the metallographic examination showed severe carburization of Type 430 stainless steel at 1700°F and slight carburization of Type 316 stainless steel at 1400°F.

Diffraction patterns indicated that the corrosion product present on the surface of Types 430 and 316 stainless steel was a mixture of $(Cr, Fe)_2O_3$ and spinel. Weight gain versus time data are plotted in

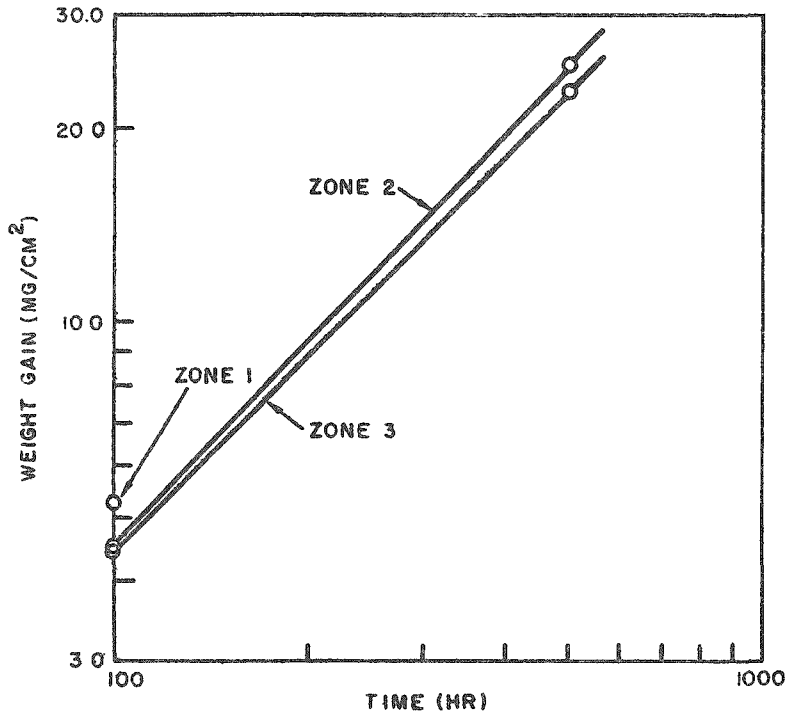

Fig. 11--Weight gain versus time for niobium in helium + 10^{-2} atm ($P_{CO} + 2P_{CO_2}$) at 1700°F

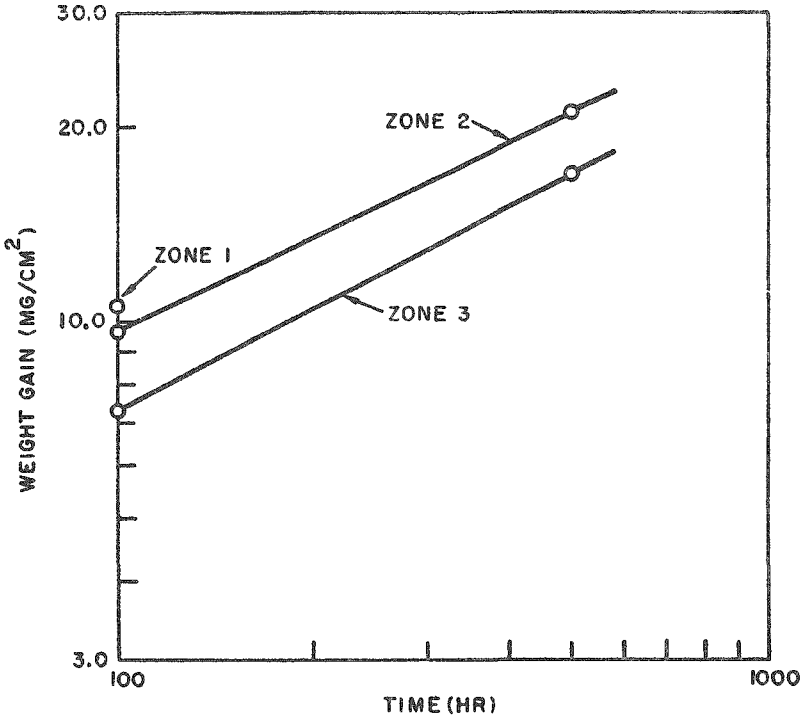

Fig. 12--Weight gain versus time for niobium + 1% Zr in helium + 10^{-2} atm ($P_{CO} + 2P_{CO_2}$) at 1700°F

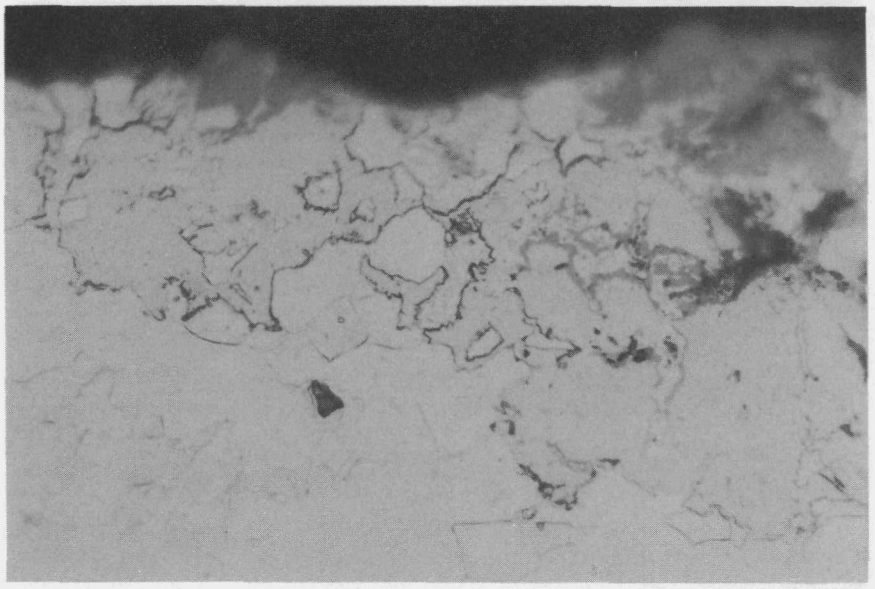

Fig. 13--Photomicrograph of niobium + 1% Zr exposed for 100 hr at 1700°F in helium + 10^{-2} atm ($P_{CO} + 2P_{CO_2}$)--penetration, 12.0 mils; corrosion products: NbC, NbO, NbO_2, Nb_2O_5 (500×)

Figs. 14 and 15. Metallographic examination of the corrosion products formed on Type 316 stainless steel revealed pits 4 mils deep after 500 hr at 1700°F (see Fig. 16).

Inconel and Inconel X showed no metallographic evidence of carburization at 1700°F; however, the carbon analysis before and after exposure indicated that a small amount of carbon had been picked up during the 500-hr exposure at 1700°F. An Inconel X specimen exposed for 500 hr at 1320°F showed definite metallographic evidence of carburization (see Fig. 17). Both of these nickel-base alloys formed surface oxides containing Cr_2O_3 and spinel, which tended to penetrate intergranularly. The thickest layers were formed on Inconel X (see Fig. 18). Weight gains after exposure are plotted in Fig. 19.

"A" nickel and Monel were affected very little by exposure in this

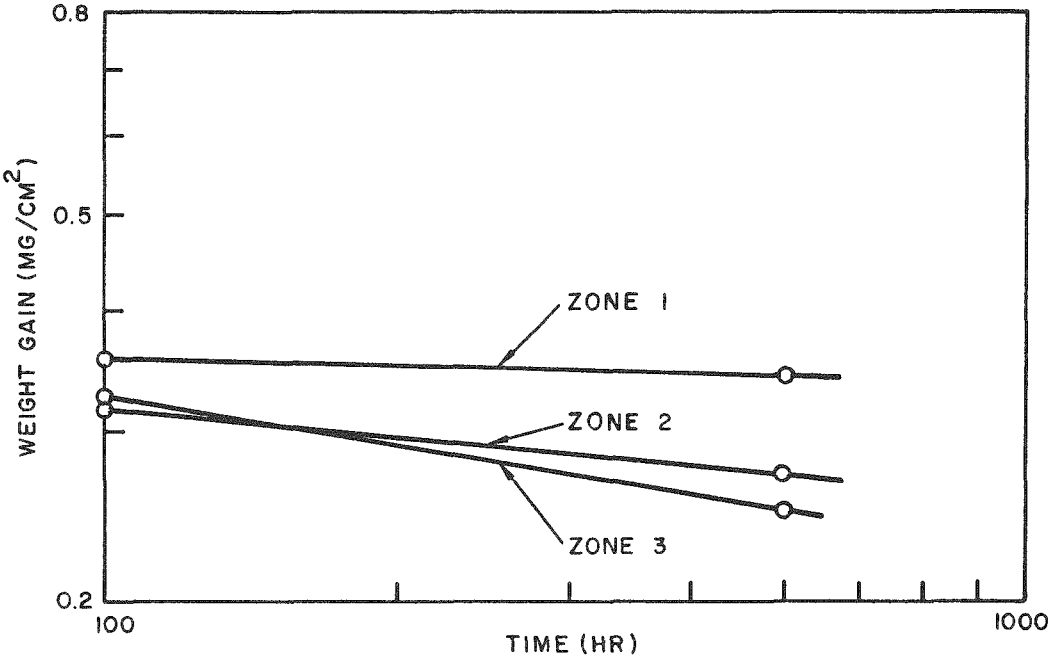

Fig. 14--Weight gain versus time for Type 316 stainless steel in helium + 10^{-2} atm ($P_{CO} + 2P_{CO_2}$) at 1700°F

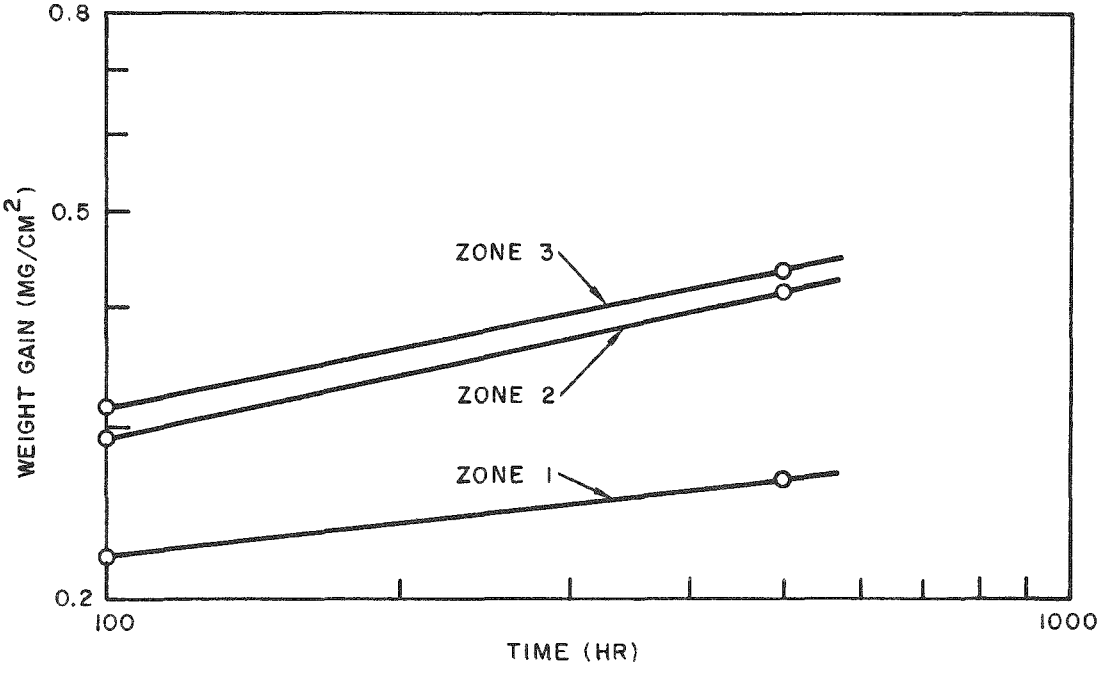

Fig. 15--Weight gain versus time for Type 430 stainless steel in helium + 10^{-2} atm ($P_{CO} + 2P_{CO_2}$) at 1700°F

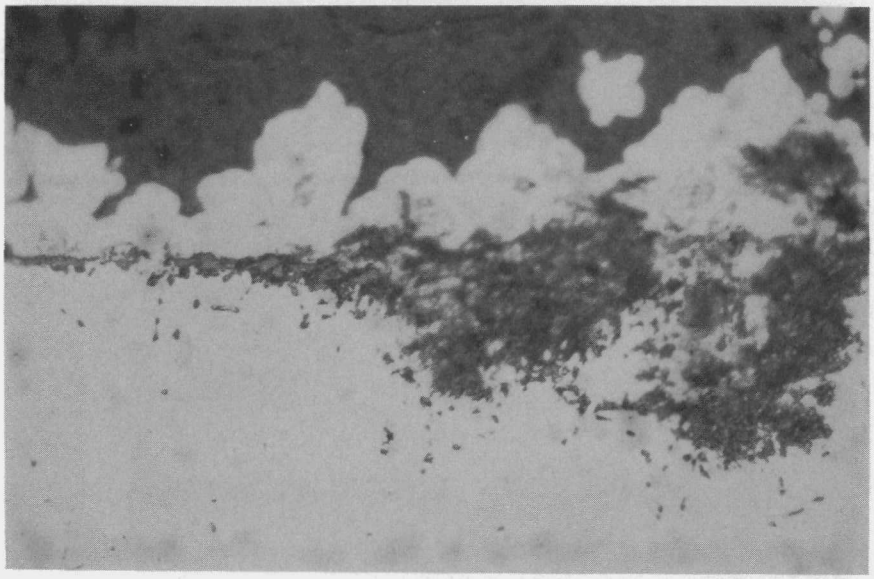

Fig. 16--Photomicrograph of Type 316 stainless steel exposed for 500 hr at 1700°F in helium + 10^{-2} atm ($P_{CO} + 2P_{CO_2}$)--penetration, 4.0 mils; corrosion product: spinel (500×)

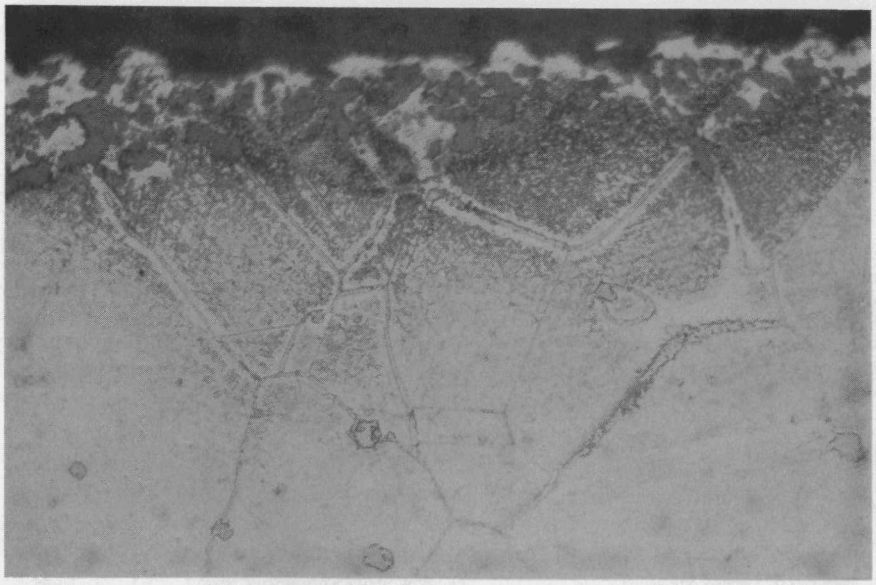

Fig. 17--Photomicrograph of Inconel X exposed for 500 hr at 1320°F in helium + 10^{-2} atm ($P_{CO} + 2P_{CO_2}$)--carburization 6.0 mils (500×)

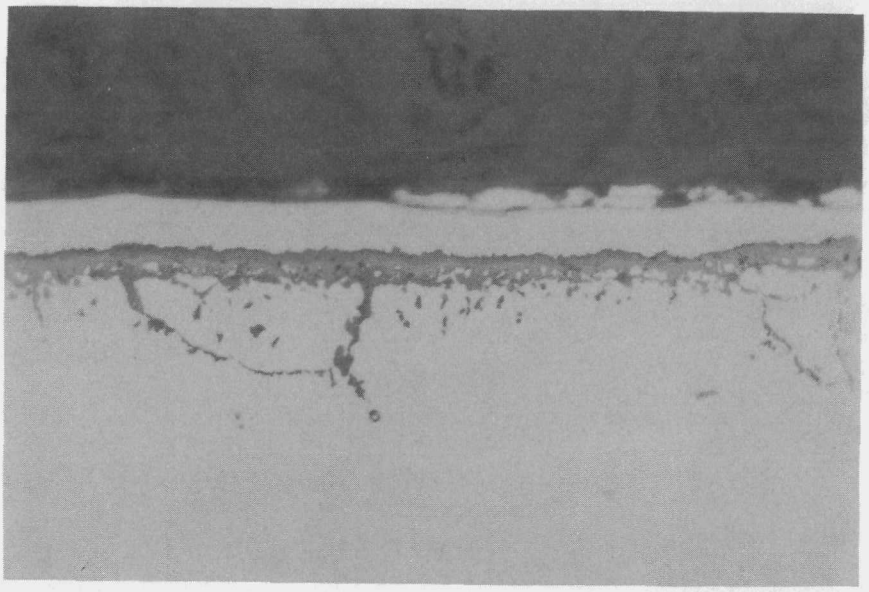

Fig. 18--Photomicrograph of surface oxide formed on Inconel X in 500 hr at 1700°F in helium + 10^{-2} atm ($P_{CO} + 2P_{CO_2}$)--corrosion products: spinel, and $(Fe,Cr)_2O_3$; penetration, 1.8 mils (500×)

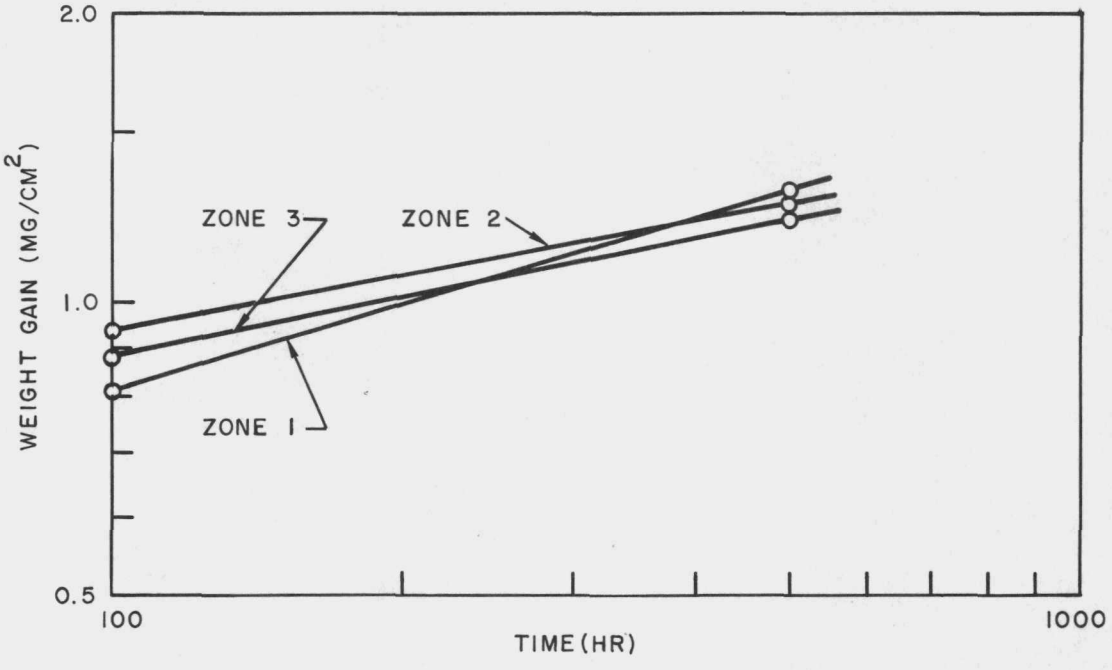

Fig. 19--Weight gain versus time for Inconel X in helium + 10^{-2} atm ($P_{CO} + 2P_{CO_2}$) at 1700°F

environment. No corrosion products were formed and metallographic examination revealed no significant attack.

No carbon transport was observed at this $CO-CO_2$ level.

Exposure in 1 atm Carbon Monoxide

The exposures in 1 atm of flowing carbon monoxide were carried out with the reaction chamber in a temperature gradient from 1700° to 150°F in the absence of graphite. This was done primarily to study the catalytic disproportionation of carbon monoxide on the surface of heat-resistant alloys. The results indicate that the low-alloy steels were most effective in catalyzing the disproportionation. A summary of the results is given in Table 5. Above 1000°F these steels were covered with a thick coat of sooty graphite. Examples of this deposit on two low-alloy steels are shown in Figs. 20a and b. The nature of the carbon deposit is illustrated in the photomicrograph of Fig. 21.

Types 430 and 316 stainless steel were much less effective catalysts than low-alloy steel. Type 430 stainless steel, after 500 hr in flowing carbon monoxide, acquired a very slight sooty surface deposit at 1550°F, whereas specimens exposed at 820°, 1300°, and 1480°F had no graphite deposited on them (see Fig. 22a). At 1370°F and above, spinel and Cr_2O_3 were identified on the surface of Type 430 stainless steel and carburization occurred. Type 316 stainless steel accumulated a small amount of graphite on the surface after 500 hr at 1250°F and 1610°F (see Fig. 22b). Surface oxides that formed on specimens exposed at 1130°F and above were identified as spinel and Cr_2O_3. Specimens exposed at 1250°F and above were carburized.

At 1390°F and above, thin, adherent graphite deposits ranging from 4 to 7 mg/cm^2 were formed on "A" nickel and Monel (see Table 5 and Figs. 23a and b). Metallographic examination of Monel exposed at 1380° and 1470°F revealed an intimately bonded graphite layer on the surface which penetrated to a maximum depth of 2.0 mils in 500 hr. A

Table 5

SUMMARY OF RESULTS FOR IRON- AND NICKEL-BASE ALLOYS EXPOSED TO 1 ATM CO

Material	Time (hr)	Temp. (°F)	Penetr. (mils)	Per cent Carbon		Corrosion Products	Weight Change (mg/cm^2)	Remarks
				Initial	Final			
C-1/2 Mo	500	1550	>30	0.12	------	Graphite, carbides	+24.9	Completely carburized; 50-mil graphite deposit
	500	1430	>30	0.12	2.07	Graphite, carbides	--------	Completely carburized; 30-mil graphite deposit
	500	1270	>30	0.12	0.268	Graphite, carbides	+1.87	Completely carburized; 0.5-mil graphite deposit
	500	300	<0.1	0.12	0.012	None	-0.02	
1/4 Cr	500	1590	>30	0.10	6.21	Graphite, carbides	+20.0	Completely carburized; 10-mil graphite deposit
	500	1450	>30	0.10	2.98	Graphite, carbides	>+20.0	Completely carburized; 10-mil graphite deposit
	500	1110	<0.1	0.10	0.18	None	+0.58	
	500	470	<0.1	0.10	0.098	None	+0.01	
	500	180	<0.1	0.10	0.11	None	+0.02	
1-1/4 Cr–1/2 Mo	500	1600	>30	0.09	10.6	Graphite, carbides	>+20	Completely carburized; 7.0-mil graphite deposit
	500	1290	>30	0.09	2.31	Graphite, carbides	>+20	Completely carburized; 10.0-mil graphite deposit
	500	800	<0.1	0.09	0.152	None	+0.08	
	500	130	<0.1	0.09	0.094	None	+0.01	
2-1/4 Cr–1 Mo	100	1610	>30	0.09	3.61	Graphite, carbides	--------	Completely carburized
	100	1250	2.0	0.09	0.148	None	--------	Grain-boundary carburization
	100	810	<0.1	0.09	0.09	None	--------	
	100	130	<0.1	0.09	0.094	None	--------	
5 Cr–1/2 Mo	500	1510	>30	0.12	------	Graphite, carbides	--------	Completely carburized
	500	1440	<0.1	0.12	0.22	None	+1.01	
	500	970	<0.1	0.12	0.12	None	+0.07	
	500	200	<0.1	0.12	0.13	None	+0.03	

Table 5--continued

Material	Time (hr)	Temp. (°F)	Penetr. (mils)	Per cent Carbon		Corrosion Products*	Weight Change (mg/cm^2)	Remarks
				Initial	Final			
9 Cr–1 Mo	500	1570	>30	0.08	------	Graphite, carbides	--------	Completely carburized; 50-mil graphite deposit
	500	1300	<0.1	0.08	0.12	None	+1.3	
	500	950	<0.1	0.08	0.11	None	+0.04	
	500	170	<0.1	0.08	0.086	None	+0.01	
430 SS	500	1540	>30	0.08	0.18	$(Spinel)_s, (Cr_2O_3)_w$	+1.0	Completely carburized
	500	1300	>30	0.08	0.24	None	+2.0	Completely carburized
	500	1370	<0.1	0.08	0.095	$(Spinel)_s, (Cr_2O_3)_w$	+0.01	
	500	820	<0.1	0.08	0.091	None	+0.02	
	500	190	<0.1	0.08	0.07	None	-0.01	
316 SS	500	1580	10.0	0.045	0.30	$(Spinel)_s$	+1.6	Carburized
	500	1350	5.0	0.045	0.17	$(Spinel)_s$	+0.96	Internal oxidation
	500	1130	0.1	0.045	0.075	$(Spinel)_w, (Cr_2O_3)_w$	+0.08	
	500	870	0.1	0.045	0.044	None	+0.02	
Inconel	500	1580	>30	0.016	0.097	$(Cr_2O_3)_s$, graphite	+17.7	Completely carburized; 2.5-mil grain-boundary oxide
	500	1350	3.5	0.016	0.015	$(Spinel)_s, (Cr_2O_3)_s$	+0.90	Internal oxidation
	500	930	<0.1	0.016	0.019	None	+0.019	
	500	400	<0.1	0.016	0.015	None	+0.006	
Inconel X	500	1590	1.8	0.035	0.086	$(Spinel)_s, [(Cr, Fe)_2O_3]_s$	+1.57	Internal oxidation
	500	1390	<0.1	0.035	0.030	None	+0.01	
	500	770	<0.1	0.035	0.030	None	+0.01	
	500	150	<0.1	0.035	0.044	None	+0.01	

*The subscript s is the small diffraction pattern, and w the weak diffraction pattern.

Table 5--continued

Material	Time (hr)	Temp. (°F)	Penetr. (mils)	Per cent Carbon		Corrosion Products	Weight Change (mg/cm^2)	Remarks
				Initial	Final			
"A" Nickel	500	1600	>30	0.011	0.52	Graphite	+4.30	Massive graphite precipitate in metal
	500	1020	<0.1	0.011	0.078	None	+0.1	
	500	550	<0.1	0.011	0.083	None	0.000	
	500	120	<0.1	0.011	0.076	None	0.000	
Monel	500	1500	1.0	0.096	0.35	Graphite	+4.0	
	500	1470	2.0	0.096	1.08	Graphite	+17.1	
	500	1380	2.0	0.096	1.15	Graphite	+16.9	
	500	860	<0.1	0.096	0.084	None	+0.013	
	500	250	<0.1	0.096	0.081	None	+0.02	

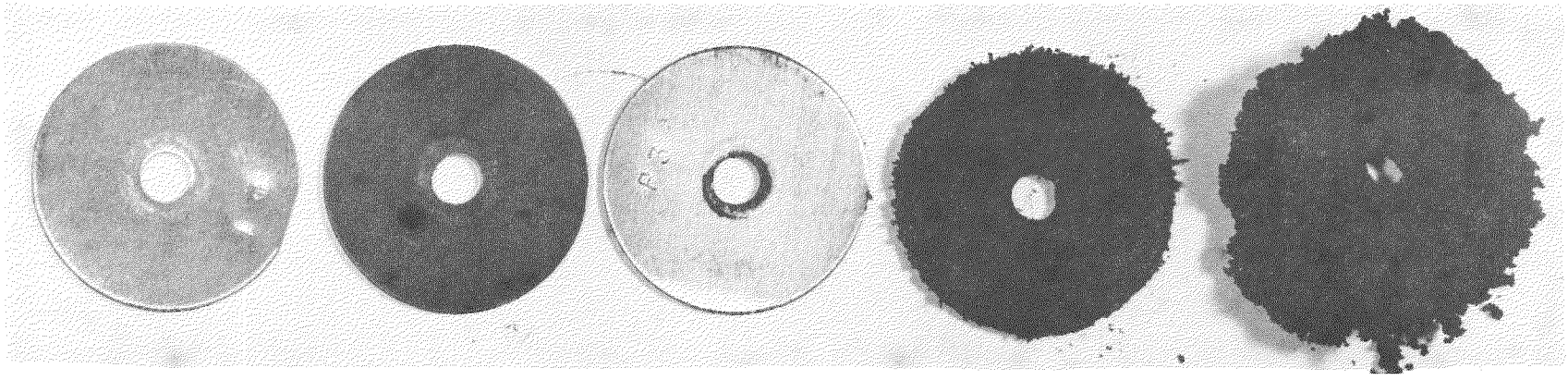

125°F 480°F 980°F 1600°F 1390°F

(a)

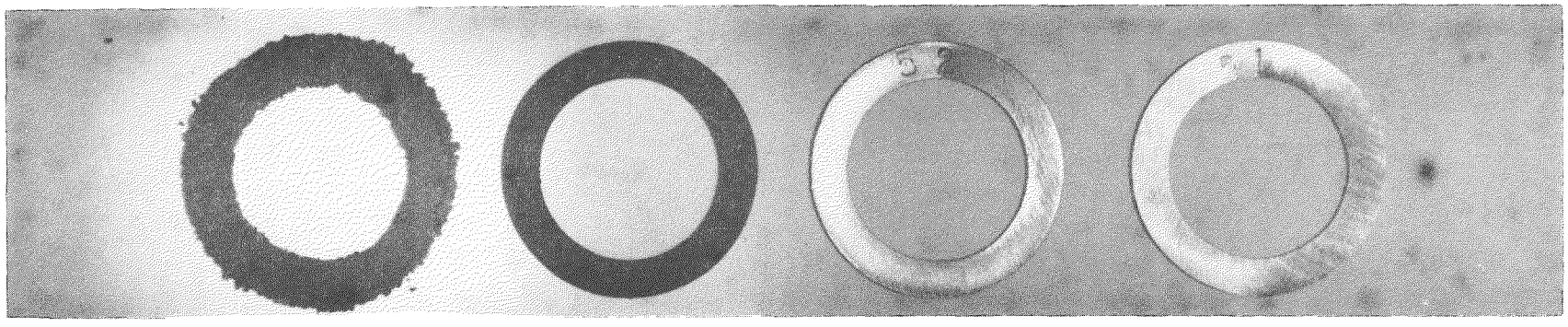

1510°F 1440°F 840°F 220°F

(b)

Fig. 20--Steel samples exposed to 1 atm of flowing CO: (a) Croloy pressure-vessel steel exposed for 500 hr; (b) steel (5 Cr–1/2 Mo) sections exposed for 100 hr

similar surface layer developed on the "A" nickel specimens and, in addition, the specimens exposed at 1600°F developed a massive graphite precipitate in the microstructure.

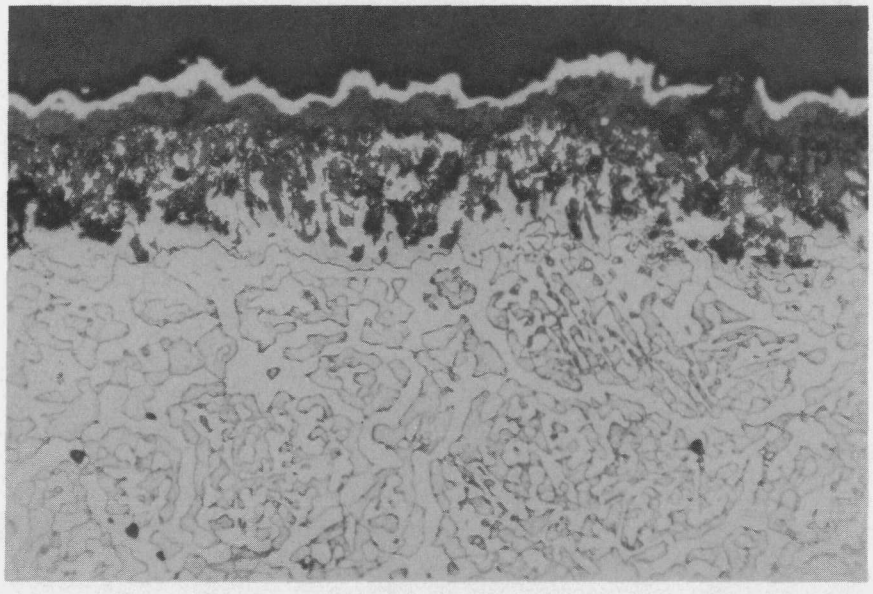

Fig. 21--Carbon deposit (preserved by electroless nickel) formed on Croloy (1/4 Cr) after 500 hr at 1450°F in 1 atm CO

Inconel did not catalyze the disproportionation of carbon monoxide at temperatures up to and including 1330°F, but at 1580°F a graphite surface layer formed with a resulting weight gain of 17.7 mg/cm^2 in 500 hr (see Fig. 24). At 1380°F two surface oxides, spinel and Cr_2O_3, were detected by X-ray diffraction, but at 1580°F only graphite and Cr_2O_3 were detected. The oxide formed at 1330°F and the graphite deposit at 1580°F are illustrated in Figs. 25 and 26.

Inconel X was particularly outstanding in <u>not</u> catalyzing the disproportionation of carbon monoxide. Specimens exposed for 500 hr in 1 atm CO are shown in Fig. 27. The specimens exposed at 770° and 1390°F were only slightly tarnished by the exposure; no surface oxide

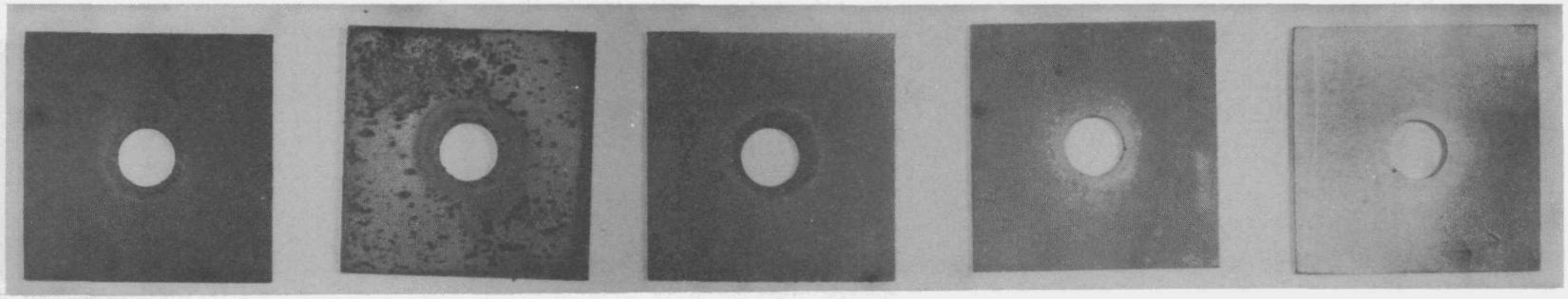

1300°F 1550°F 1480°F 820°F 200°F

(a)

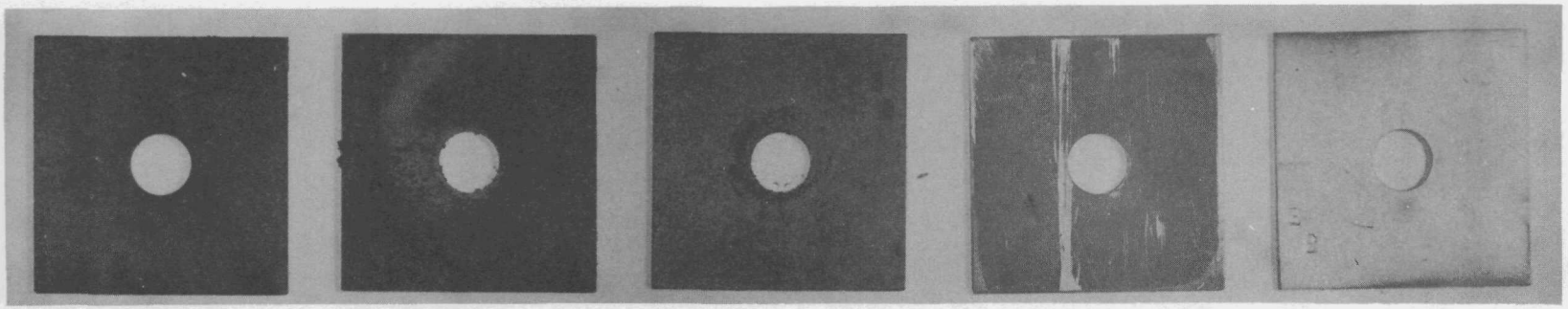

1250°F 1610°F 1130°F 680°F 140°F

(b)

Fig. 22--Stainless steel exposed to 1 atm of flowing CO for 500 hr: (a) Type 430; (b) Type 316

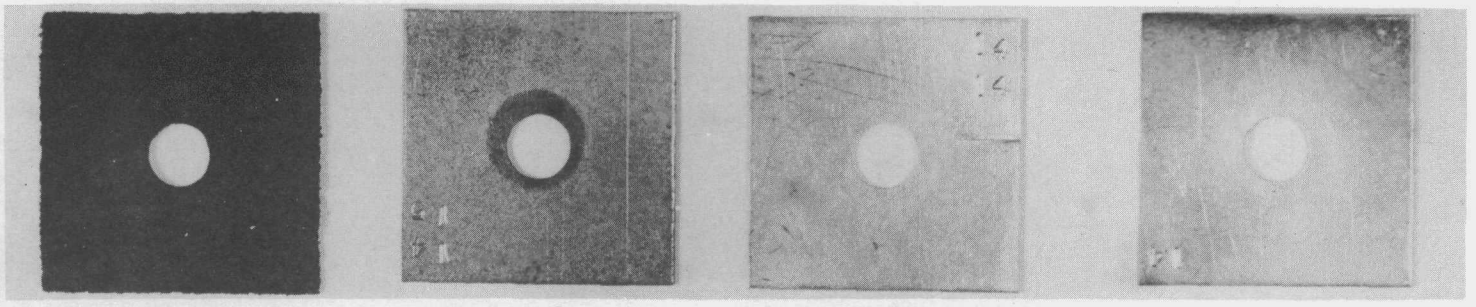

(a)

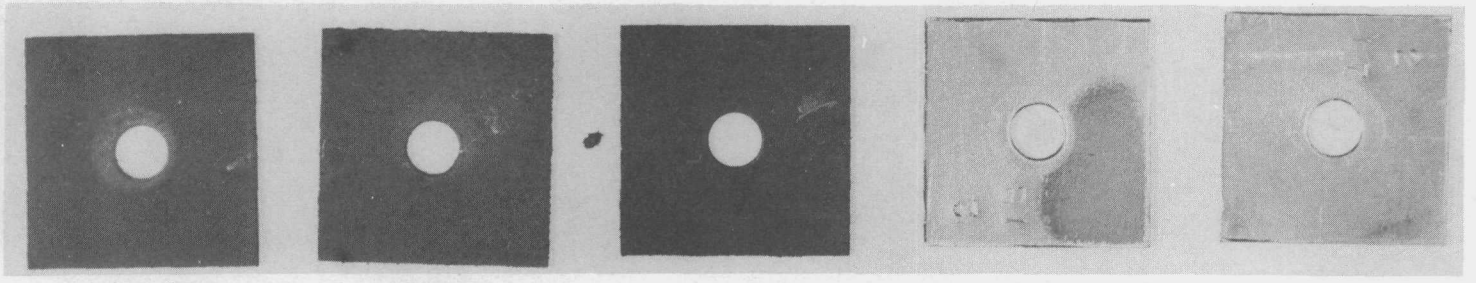

(b)

Fig. 23--Samples of nickel and Monel exposed to 1 atm of flowing CO for 500 hr: (a) nickel; (b) Monel

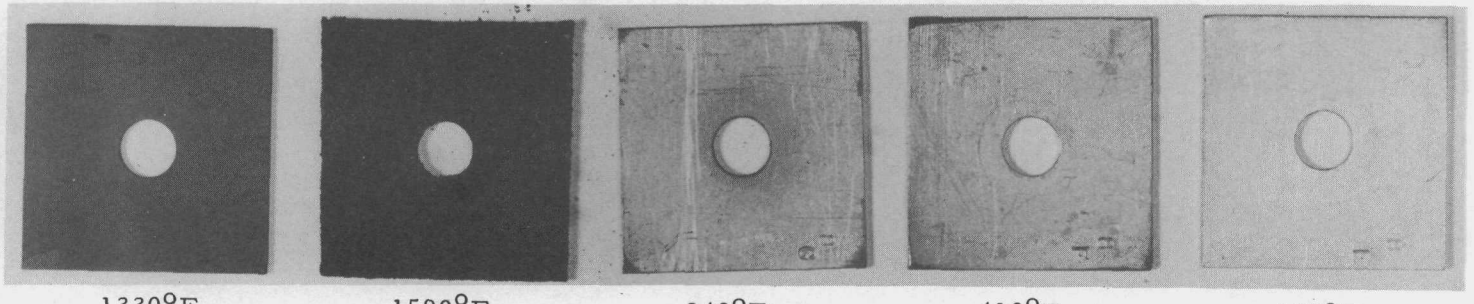

Fig. 24--Inconel exposed to 1 atm of flowing CO for 500 hr

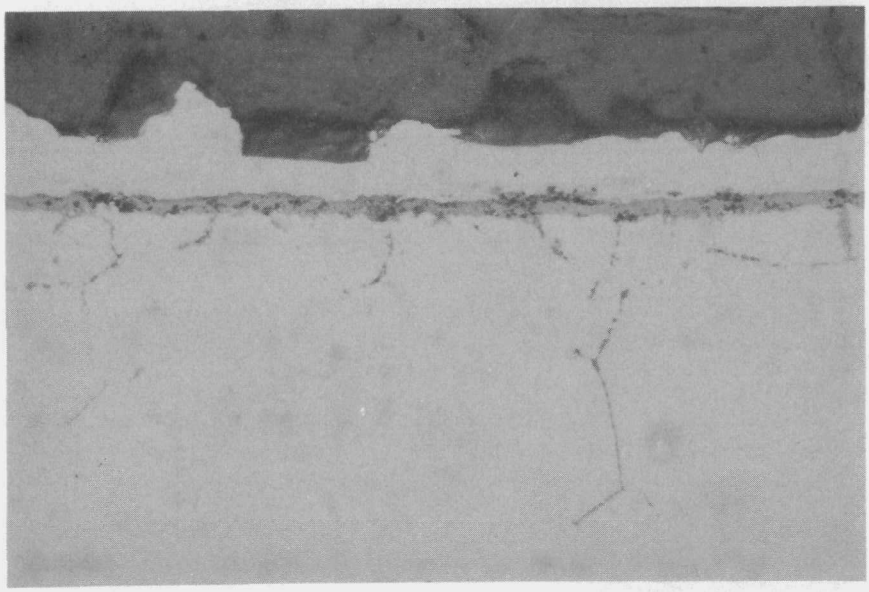

Fig. 25--Surface oxide formed on Inconel in 500 hr at 1330°F in 1 atm CO (500×)

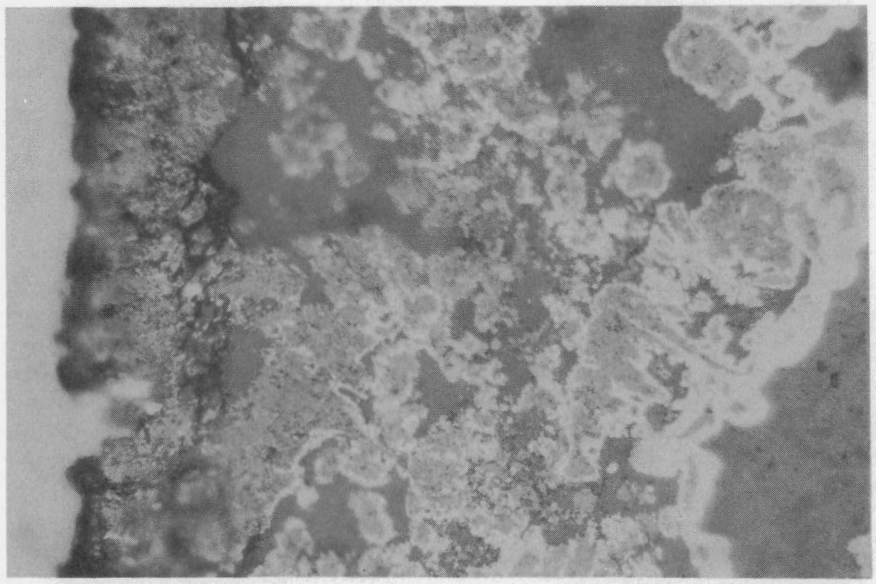

Fig. 26--Graphite deposited on Inconel in 500 hr at 1580°F in 1 atm CO (500×)

could be detected by X-ray diffraction. At 1590°F, a thick protective oxide of spinel and $(Cr, Fe)_2O_3$ was formed, which was effective in preventing the catalytic decomposition of carbon monoxide on the metal surface (see Fig. 28).

The results of exposure of niobium and five niobium-base alloys to 1 atm of flowing carbon monoxide have been summarized in Table 6. Above about 700°F a thin surface layer, identified by X-ray diffraction as a mixture of carbides, developed on all alloys. The carbide layer in no case exceeded 0.2 mil in thickness and was not accompanied by embrittlement. The alloys containing 5% zirconium and 5% or 10% titanium exhibited, in addition to the thin carbide layer, a zone on the surface which appeared to be a contaminated solid solution. The 8% and 10% titanium alloys gained the most weight during the exposure, though these weight gains were small--2 mg/cm^2 in 500 hr at 1600°F.

No disproportionation of carbon monoxide on niobium or any of its alloys was observed. Figure 29 shows the niobium specimens (typical also of the alloys) exposed to 1 atm CO at the indicated temperatures.

Exposure in 0.5 atm CO + 0.5 atm H_2

The exposures in 0.5 atm CO + 0.5 atm H_2 were conducted in a temperature gradient of 1700° to 150°F. The purpose of these tests was to determine the effect of hydrogen on the decomposition of carbon monoxide on various reactor materials. Table 7 summarizes the results of these tests.

The materials most effective in catalyzing carbon deposition below 1000°F in H_2 + CO were the low-alloy steels, Inconel X, Inconel 702, and Type 316 stainless steel; nickel and Monel were somewhat less effective catalysts. Examples of these carbon deposits, together with weight-gain data, are illustrated in Figs. 30 through 38.

The steel most ineffective in catalyzing the carbon monoxide decomposition was Type 430 stainless steel, although above 1300°F some carbon

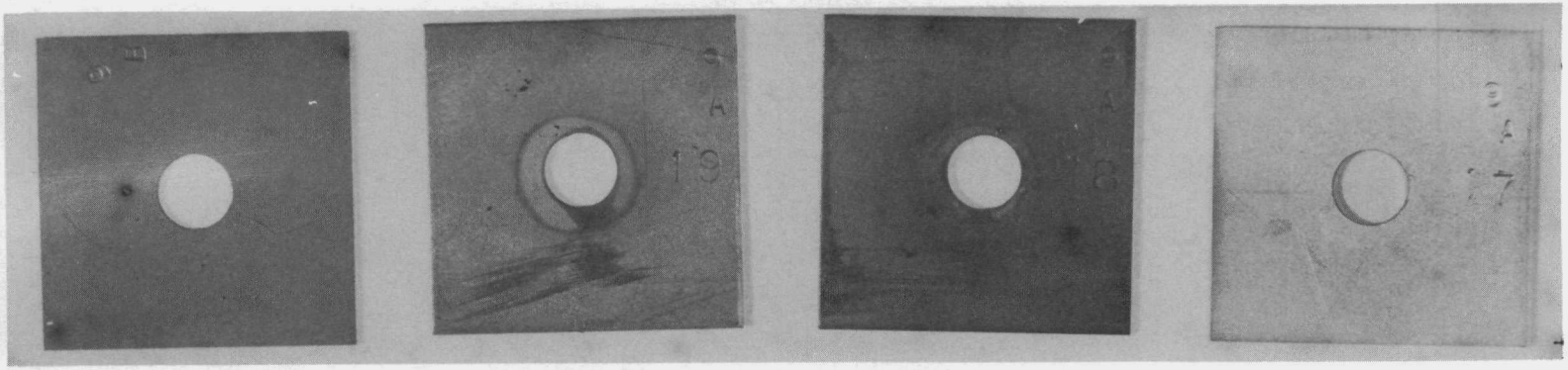

1590°F 1250°F 770°F 160°F

Fig. 27--Inconel X exposed to 1 atm of flowing CO for 500 hr

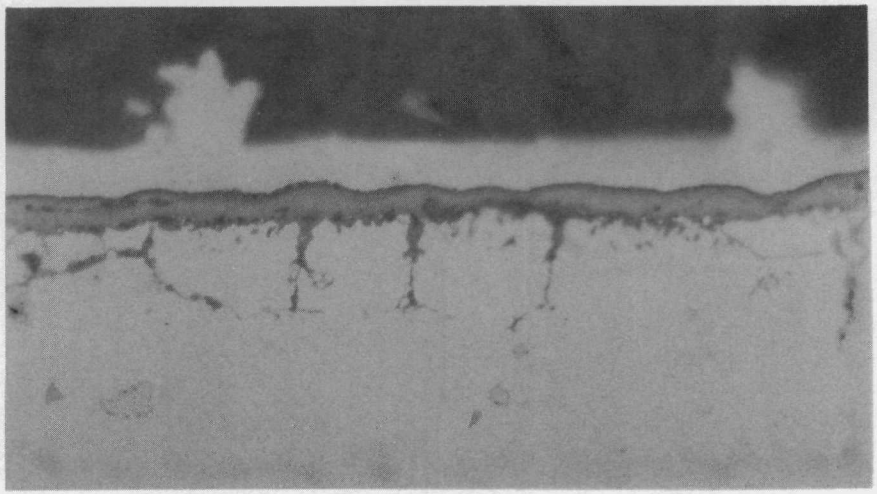

Fig. 28--Surface oxide formed on Inconel X after 500 hr in 1 atm CO at 1590°F (500×)

Table 6

SUMMARY OF RESULTS FOR NIOBIUM ALLOYS TESTED IN 1 ATM CO

Material	Time (hr)	Temp. (°F)	Penetr. (mils)	Per cent Carbon		Corrosion Products*	Weight Change (mg/cm^2)	Remarks
				Initial	Final			
Niobium	500	1450	0.2	0.001	0.040	$(NbC)_s$, $(Nb_2C)_m$	+0.300	
	500	1050	<0.1	0.001	0.023	$(Nb_2C)_w$	+0.060	
	500	530	<0.1	0.001	0.002	None	+0.033	
	500	115	<0.1	0.001	0.001	None	+0.013	
Niobium + 1% Zr	500	1620	0.2	0.004	0.068	$(NbC)_s$, $(Nb_2C)_s$	+0.80	
	500	1490	0.1	0.004	0.072	$(NbC)_s$, $(Nb_2C)_s$	+0.43	
	500	1140	0.1	0.004	0.023	$(NbC)_w$, $(Nb_2C)_w$	+0.08	
	500	630	<0.1	0.004	0.006	None	+0.04	
	500	140	<0.1	0.004	0.005	None	+0.007	
Niobium + 5% Zr	500	1610	7.0	0.020	0.137	$(NbC)_s$, $(Nb_2C)_s$	+0.36	Solid solution surface layer
	500	1410	1.5	0.020	0.070	$(NbC)_m$, $(Nb_2C)_w$	+0.66	Solid solution surface layer
	500	970	<0.1	0.020	0.061	$(NbC)_w$, $(Nb_2C)_w$	+0.09	
	500	440	<0.1	0.020	0.023	None	0.000	
	500	110	<0.1	0.020	0.021	None	-0.010	
Niobium + 5% Ti	500	1610	4.5	0.015	0.098	$(NbC)_s$, $(Nb_2C)_m$	+0.75	Solid solution surface layer
	500	1570	7.0	0.015	0.152	$(NbC)_s$, $(Nb_2C)_s$	+0.73	Solid solution surface layer
	500	1350	2.0	0.015	0.046	$(NbC)_w$, $(Nb_2C)_w$	+0.51	Solid solution surface layer
	500	890	2.0	0.015	0.019	$(NbC)_w$, $(Nb_2C)_w$	+0.062	Solid solution surface layer
	500	530	2.0	0.015	0.017	$(NbC)_w$, $(Nb_2C)_w$, $(TiC)_w$	+0.020	Solid solution surface layer

*The subscript s is the small diffraction pattern; m, the medium diffraction pattern; and w, the weak diffraction pattern.

Table 6--continued

Material	Time (hr)	Temp. (°F)	Penetr. (mils)	Per cent Carbon		Corrosion Products*	Weight Change (mg/cm^2)	Remarks
				Initial	Final			
Niobium + 8% Ti	500	1630	4.0	0.030	0.36	$(NbC)_s, (Nb_2C)_m, (TiC)_m$	+1.70	Solid solution surface layer
	500	1520	3.0	0.030	0.28	$(NbC)_s, (Nb_2C)_s, (TiC)_m$	+1.25	Solid solution surface layer
	500	1210	<0.1	0.030	0.068	$(NbC)_w, (Nb_2C)_m, (TiC)_w$	+0.22	
	500	730	<0.1	0.030	0.035	$(NbC)_w, (Nb_2C)_w, (TiC)_w$	+0.064	
	500	170	<0.1	0.030	0.033	None	+0.015	
Niobium + 10% Ti	500	1620	4.0	0.022	0.18	$(NbC)_s, (Nb_2C)_m, (TiC)_w$	+1.30	Solid solution surface layer
	500	1550	4.0	0.022	0.23	$(NbC)_s, (Nb_2C)_m, (TiC)_w$	+1.65	Solid solution surface layer
	500	1290	3.0	0.022	0.04	$(NbC)_s, (Nb_2C)_m, (TiC)_w$	+0.31	Solid solution surface layer
	500	810	1.0	0.022	0.23	$(NbC)_w, (Nb_2C)_w, (TiC)_w$	+0.07	Solid solution surface layer
	500	230	2.0	0.022	0.24	None	+0.02	Solid solution surface layer

*The subscript s is the small diffraction pattern; m, the medium diffraction pattern; and w, the weak diffraction pattern.

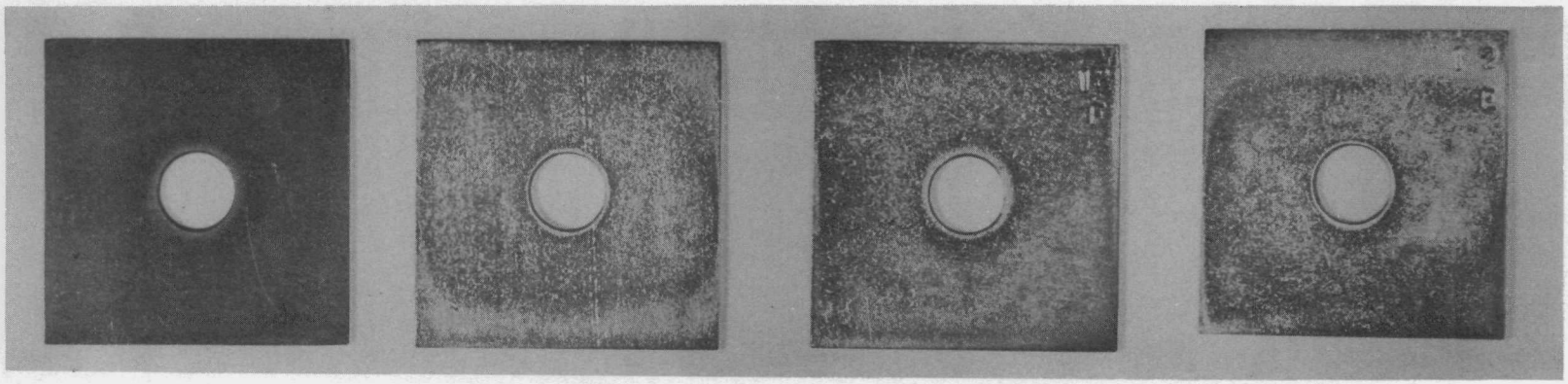

1450°F 1050°F 530°F 120°F

Fig. 29--Niobium exposed to 1 atm of flowing CO for 500 hr

Table 7

SUMMARY OF RESULTS FOR IRON- AND NICKEL-BASE ALLOYS EXPOSED TO 0.5 ATM CO + 0.5 ATM H_2

Material	Time (hr)	Temp. (^{o}F)	Penetr. (mils)	Per cent Carbon		Corrosion Products*	Weight Change (mg/cm^2)	Remarks
				Initial	Final			
316 SS	400	100	<0.2	0.045	-----	None	-0.010	
	400	400	<0.2	0.045	0.060	None	-0.010	
	400	810	<0.2	0.045	0.057	None	-0.015	
	400	910	2.0	0.045	0.27	None	0.875	Intergranular fissures
	400	1250	>30	0.045	1.21	Graphite	-8.915	Completely carburized
	400	1600	0.5	0.045	0.081	$(Spinel)_s$	0.315	Intergranular oxidation
	400	1730	1.0	0.045	0.067	$(Spinel)_s$	0.255	Intergranular oxidation
	400	1690	1.0	0.045	0.050	$(Spinel)_s$	0.260	Intergranular oxidation
430 SS	400	100	<0.2	0.08	-----	None	0.000	
	400	600	<0.2	0.08	0.062	None	-0.010	
	400	810	<0.2	0.08	0.075	None	-0.015	
	400	970	<0.2	0.08	0.075	None	-0.010	
	400	1330	<0.2	0.08	0.099	$(Spinel)_m$	0.085	
	400	1610	>30	0.08	0.157	$(Spinel)_s, (Cr_2O_3)_w$	0.335	Carburized
	400	1740	>30	0.08	0.28	$(Spinel)_s$	1.050	Carburized; 3.5-mil internal oxidation
	400	1680	>30	0.08	0.139	$(Spinel)_s$	0.275	Carburized; 1.0-mil internal oxidation
C–1/2 Mo	400	120	<0.2	0.12	0.122	None	0.118	
	400	750	<0.2	0.12	0.129	None	0.0472	
	400	830	<0.2	0.12	0.143	Graphite	0.543	
	100	990	-----	0.12	-----	Graphite	------	Heavy graphite deposit
1-1/4 Cr–1/2 Mo	400	160	<0.2	0.09	0.124	None	-0.0588	
	400	780	<0.2	0.09	0.099	None	-0.0147	
	400	850	<0.2	0.09	0.126	Graphite	4.060	

*The subscript s is the small diffraction pattern; m, the medium diffraction pattern; and w, the weak diffraction pattern.

Table 7--continued

Material	Time (hr)	Temp. (°F)	Penetr. (mils)	Per cent Carbon		Corrosion Products*	Weight Change (mg/cm^2)	Remarks
				Initial	Final			
Inconel 702	400	140	<0.2	0.02	-----	None	-0.010	
	400	760	<0.2	0.02	0.040	None	0.000	
	400	830	<0.2	0.02	0.026	None	-0.020	
	400	1100	<0.2	0.02	0.055	Graphite		
	400	1350	1.0	0.02	0.42	$(Spinel)_m$, $(Cr_2O_3)_s$, graphite		Internal oxidation
	400	1650	1.5	0.02	0.19	$(Spinel)_m$, $[(Cr, Fe)_2O_3]_s$	1.940	Internal oxidation; 2.0-mil decarburization
	400	1750	4.0	0.02	0.134	$(Spinel)_w$, $[(Cr, Fe)_2O_3]_s$	2.000	Internal oxidation; 8.0-mil decarburization
	400	1650	2.5	0.02	0.091	$(Spinel)_w$, $[(Cr, Fe)_2O_3]_s$	1.625	Internal oxidation; 3.5-mil decarburization
Inconel X	400	150	<0.2	0.035	-----	None	-0.995	
	400	780	<0.2	0.035	0.047	None	-0.010	
	400	840	<0.2	0.035	0.045	None	-0.010	
	400	1130	<0.2	0.035	0.028	Graphite	-21.53	
	400	1390	1.0	0.035	0.055	$(Spinel)_s$, $[(Cr, Fe)_2O_3]_s$	0.620	Intergranular oxidation
	400	1680	2.5	0.035	0.085	$(Spinel)_s$, $[(Cr, Fe)_2O_3]_s$	1.880	Intergranular oxidation
	400	1750	2.5	0.035	0.071	(Spinel)	2.025	Intergranular oxidation
	400	1600	2.0	0.035	0.09	$(Spinel)_s$, $[(Cr, Fe)_2O_3]_s$	1.345	Intergranular oxidation
Nickel	400	200	<0.2	0.011	-----	None	0.000	
	400	790	<0.2	0.011	0.096	None	-0.050	
	400	860	<0.2	0.011	0.04	None	-0.045	
	400	1180	>30	0.011	0.14	Graphite		Graphite precipitation in metal, 2.0-mil graphite deposit
	400	1510	>30	0.011	0.25	Graphite		Graphite precipitation in metal; 14.0-mil graphite deposit
	400	1710	>30	0.011	0.27	Graphite	8.570	Graphite precipitation in metal; 3.0-mil graphite deposit
	400	1750	>30	0.011	0.74	$(Graphite)_m$	4.262	Graphite precipitation in metal; 3.5-mil graphite deposit

*The subscript s is the small diffraction pattern, m, the medium diffraction pattern, and w, the weak diffraction pattern.

Table 7--continued

Material	Time (hr)	Temp. (°F)	Penetr. (mils)	Per cent Carbon		Corrosion Products*	Weight Change (mg/cm^2)	Remarks
				Initial	Final			
Monel	400	220	<0.2	0.096	-----	None	0.000	
	400	800	<0.2	0.096	0.09	None	0.005	
	400	880	<0.2	0.096	0.08	None	0.030	
	400	1220	1 to 3	0.096	0.14	Graphite		Graphite penetration; 12.0-mil graphite deposit
	400	1570	1 to 4	0.096	0.25	Graphite		Graphite penetration; 15.0-mil graphite deposit
	400	1720	1 to 5	0.096	0.15	Graphite	31.735	Graphite penetration; 10.0-mil graphite deposit
	400	1730	1 to 5	0.096	0.17	$(Graphite)_s$	28.100	Graphite penetration; 14.0-mil graphite deposit

*The subscript s is the small diffraction pattern.

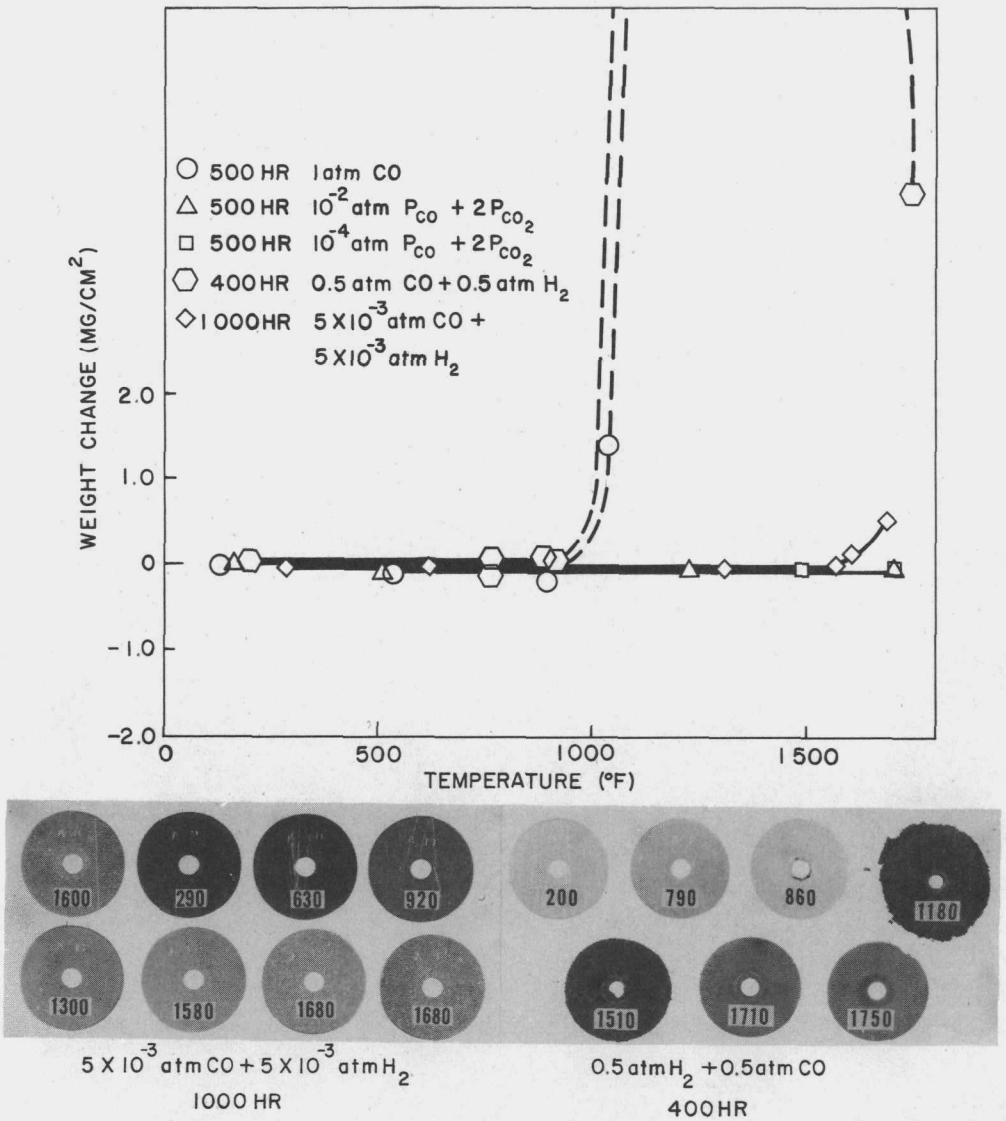

Fig. 30--Nickel specimen tested in two partial pressures of H_2 + CO, together with weight change versus temperature (numbers on specimens indicate temperature)

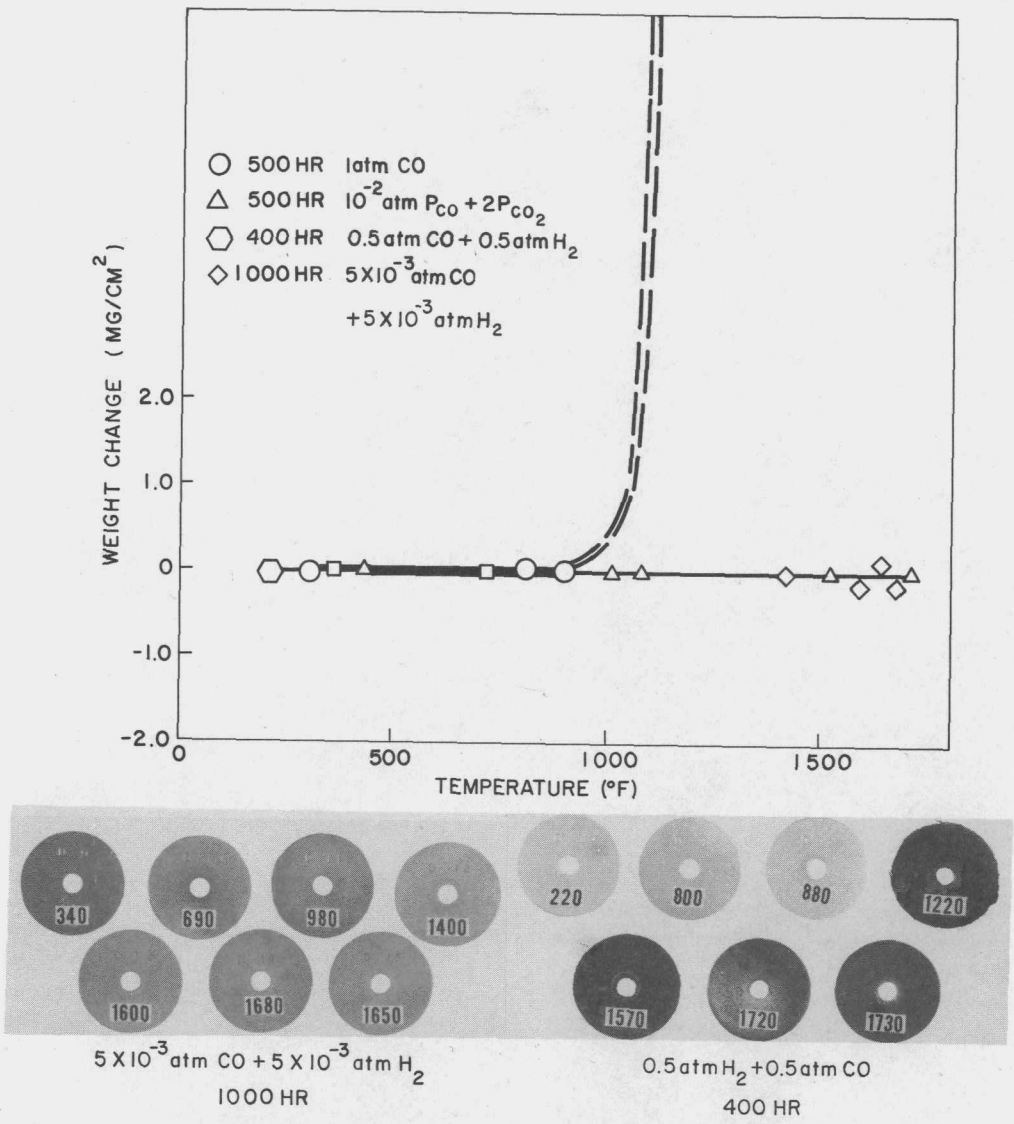

Fig. 31--Monel specimens tested in two partial pressures of H_2 + CO, together with weight change versus temperature (numbers on specimens indicate temperature)

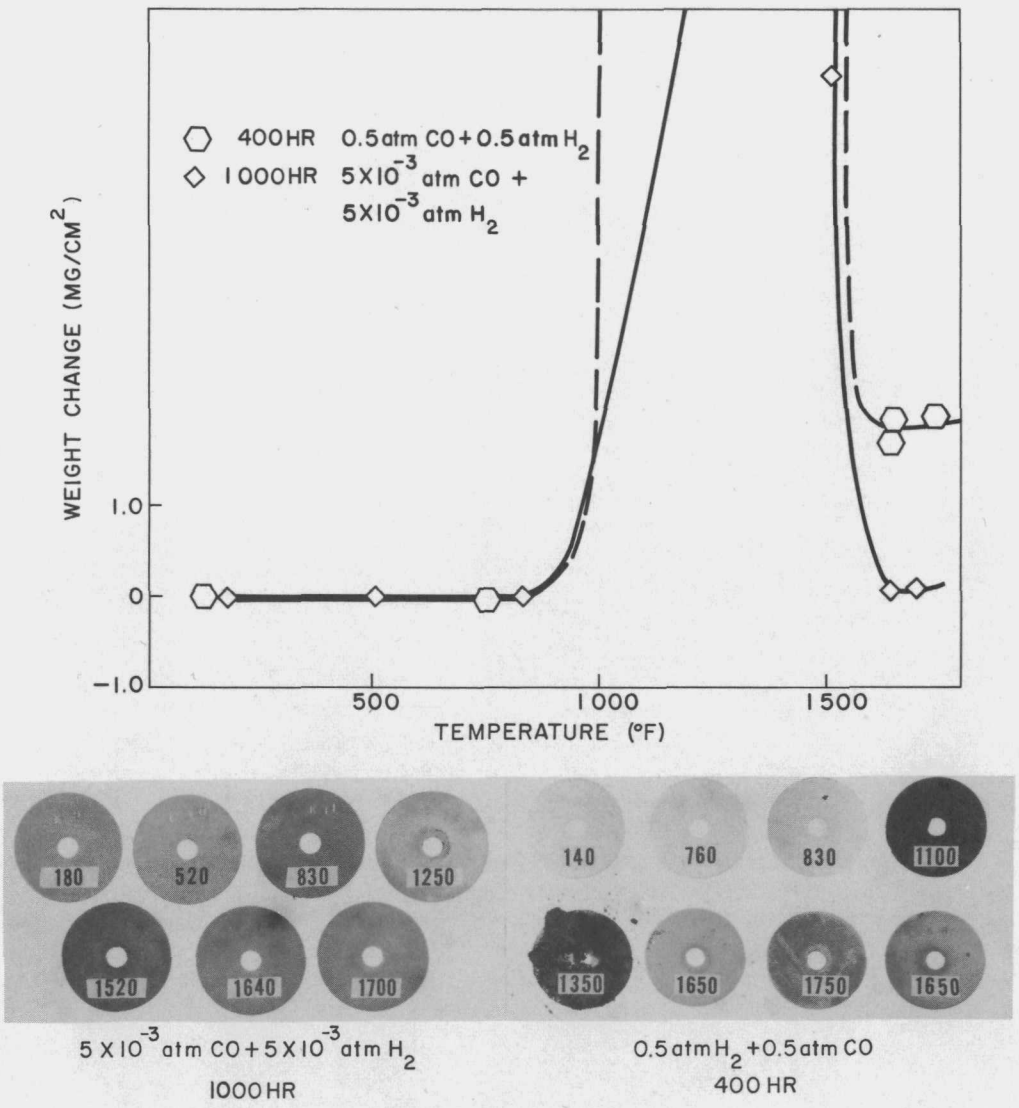

Fig. 32--Inconel 702 specimens tested in two partial pressures of H_2 + CO, together with weight change versus temperature (numbers on specimens indicate temperature)

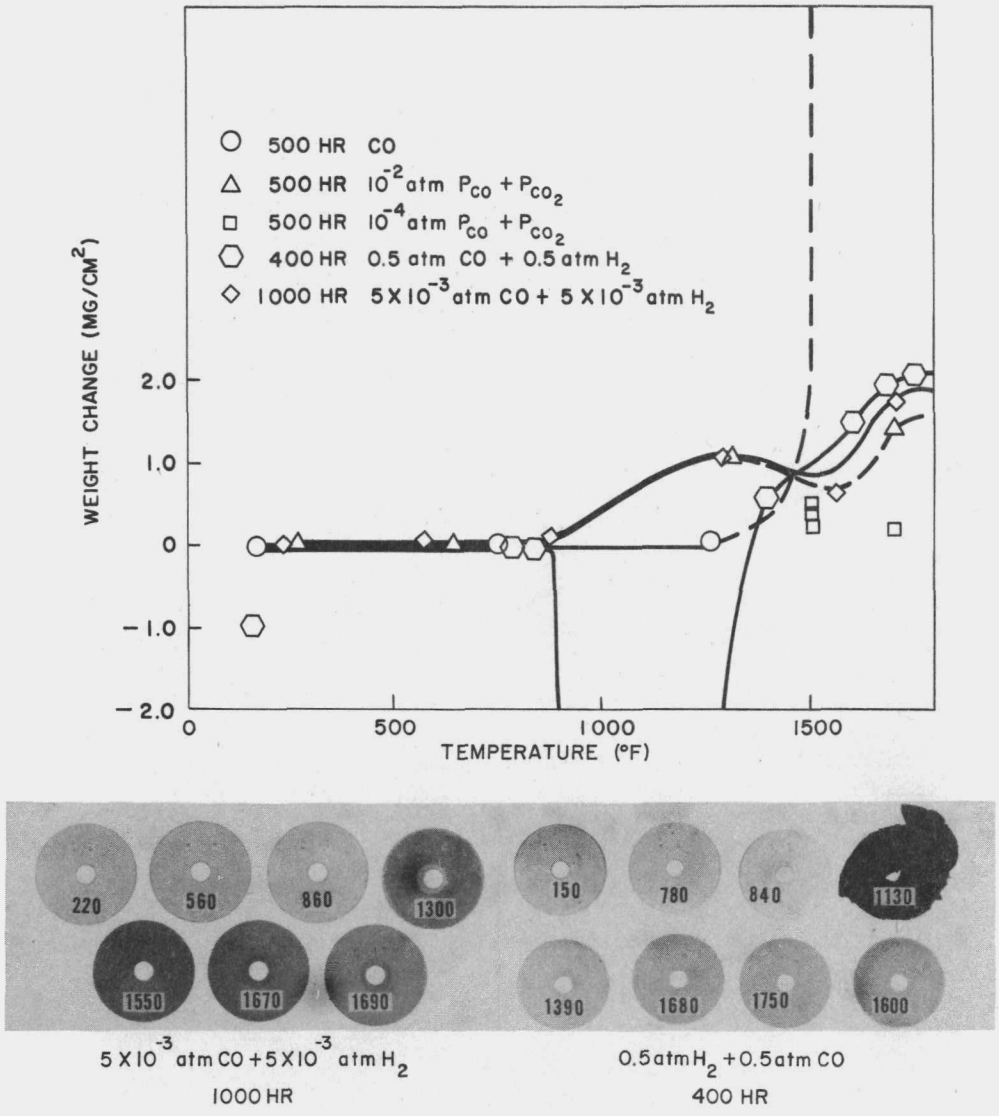

Fig. 33--Inconel X specimens tested in two partial pressures of H_2 + CO, together with weight change versus temperature (numbers on specimens indicate temperature)

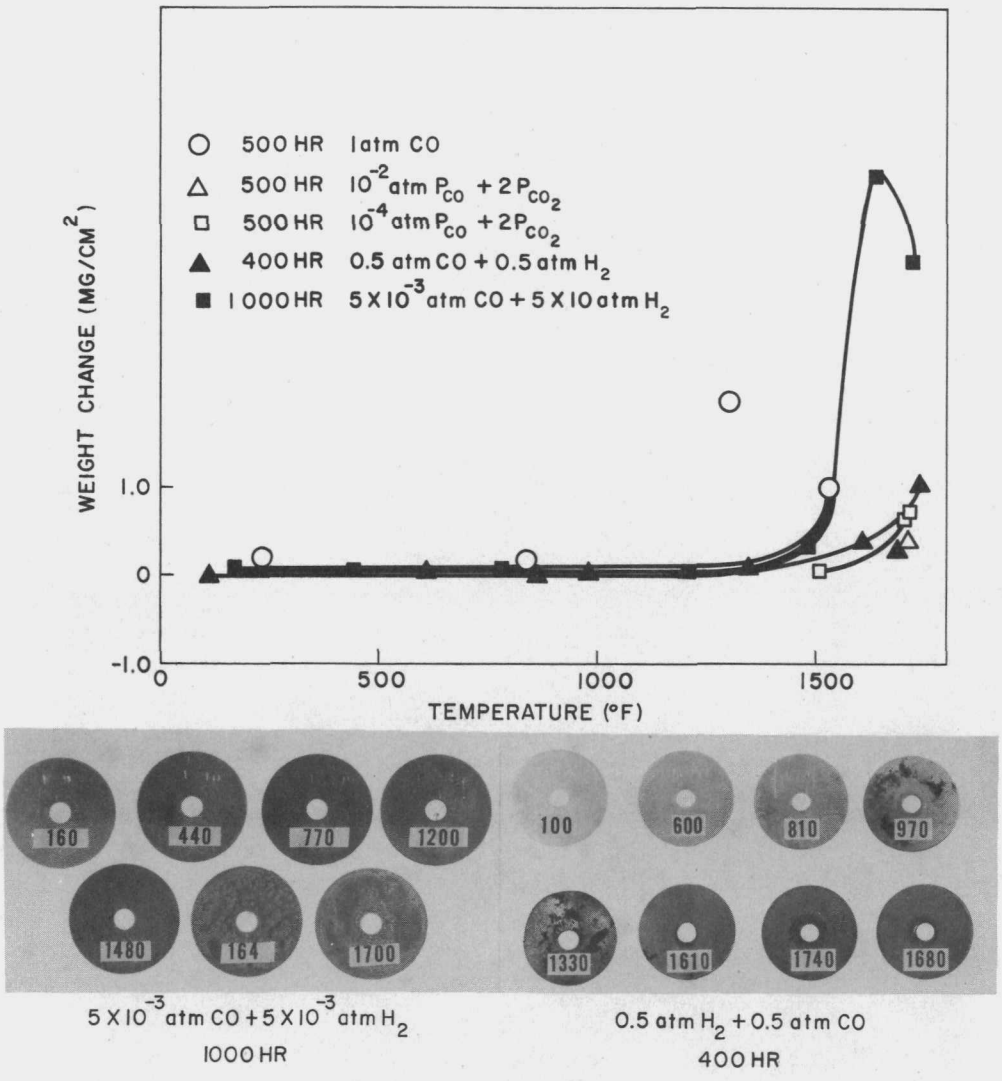

Fig. 34--Type 430 stainless steel specimens tested in two partial pressures of H_2 + CO, together with weight change versus temperature (numbers on specimens indicate temperature)

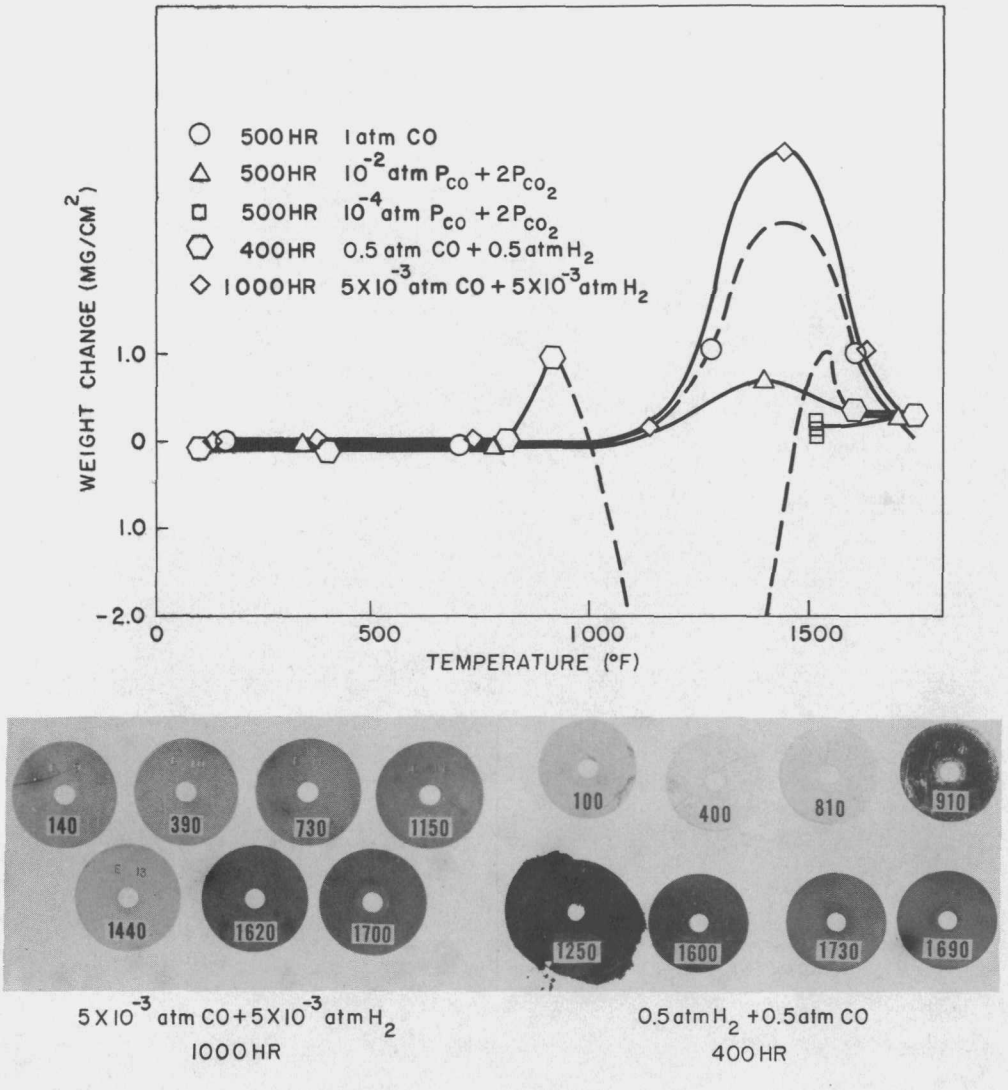

Fig. 35--Type 316 stainless steel specimens tested in two partial pressures of H_2 + CO, together with weight change versus temperature (numbers on specimens indicate temperature)

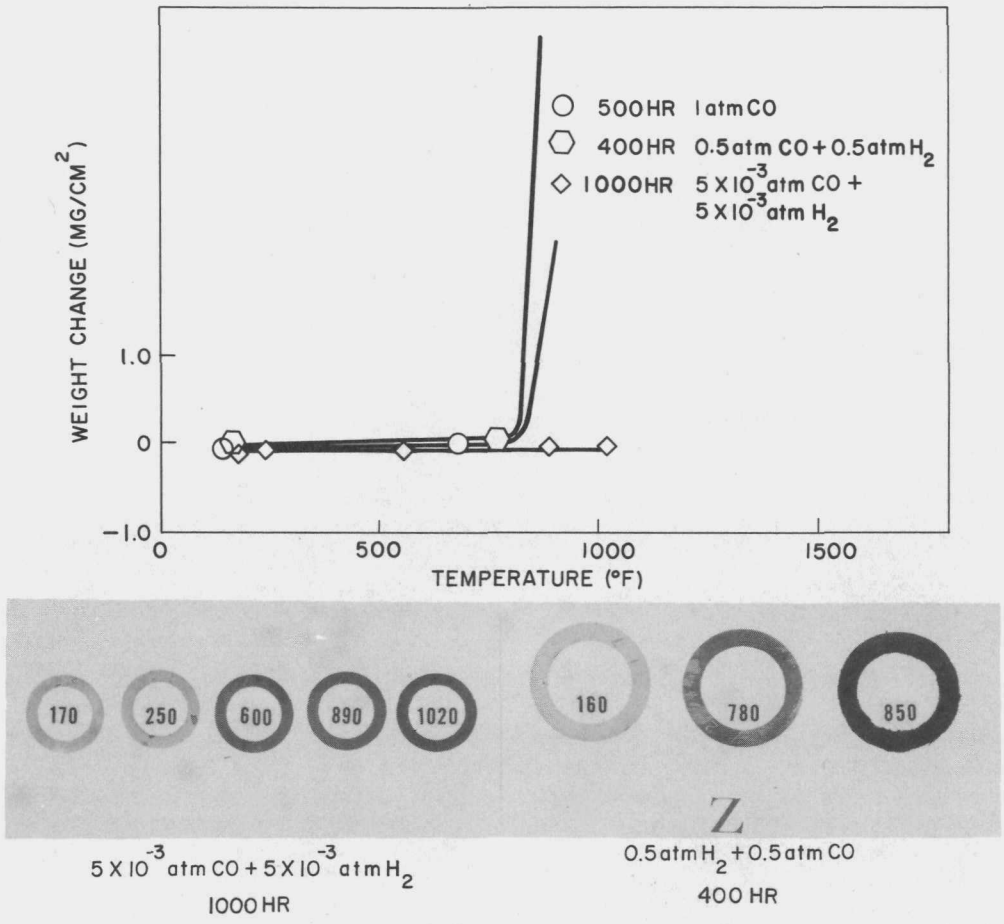

Fig. 36--Steel (1-1/4 Cr—1/2 Mo) specimens tested in two partial pressures of H_2 + CO, together with weight change versus temperature (numbers on specimens indicate temperature)

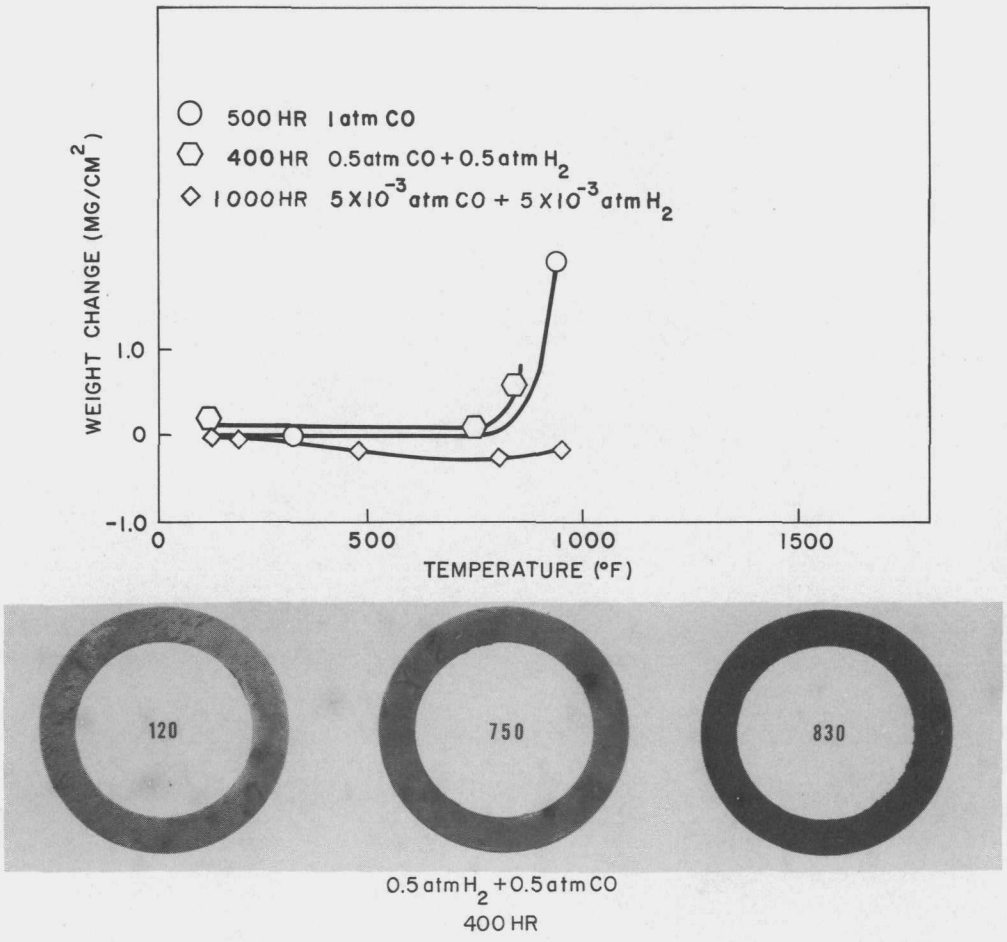

Fig. 37--Steel (C—1/2 Mo) specimens tested in two partial pressures of H_2 + CO, together with weight change versus temperature (numbers on specimens indicate temperature)

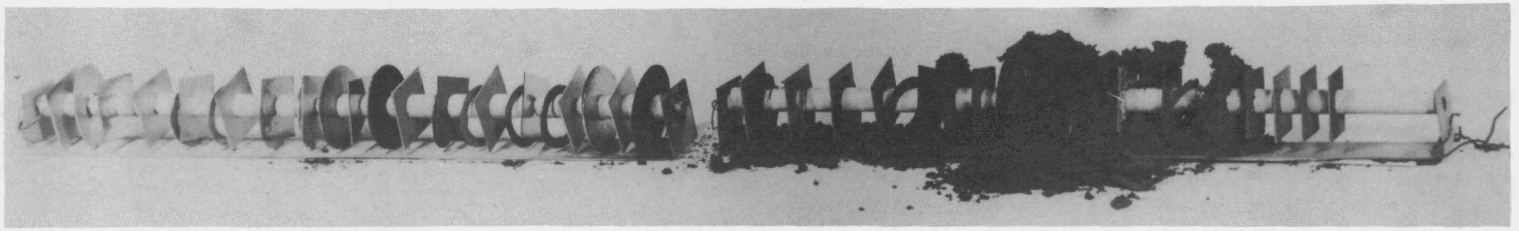

500° 1000° 1500° 1200°

(a)

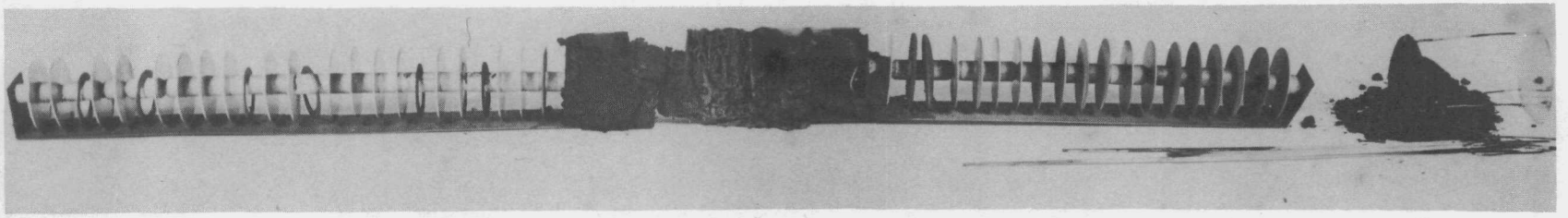

500° 1000° 1500° 1200°

(b)

Fig. 38--Samples of iron and nickel alloys (a) tested in a temperature gradient for 500 hr in 1 atm CO, (b) tested in a temperature gradient for 400 hr in 0.5 atm CO + 0.5 atm H_2

deposition occurred. At 1300°F carbon whiskers grew from the numbers stamped on the specimens, but at 1740°F carburization penetrated 3.5 mils in 400 hr.

At 1250°F, Type 316 stainless steel catalyzed decomposition producing a carbon growth from the metal surface that contained about 5 wt-% iron; the metal specimen was completely carburized. The catalyzation of carbon monoxide decomposition of Type 316 stainless steel extended from approximately 900° to 1500°F, but from 1600° to 1730°F surface oxides (spinels) nearly 1 mil thick were formed.

The carbon—1/2 Mo steel and 1-1/4 Cr—1/2 Mo both produced rapid growth of carbon on their surfaces above 800°F in the 0.5 atm CO + 0.5 atm H_2 (see Figs. 37 and 38). Near 1000°F, the carbon—1/2 Mo steel catalyzed such rapid growth that it was removed from the test after 100 hr.

Carbon was deposited on the surface of Inconel X and Inconel 702 at 1100°F, but at 1350°F and higher these two alloys were intergranularly oxidized (see Fig. 39a and b). Corrosion products formed at high temperature consisted of spinel and $(Cr, Fe)_2O_3$.

At 1200°F and above, carbon was deposited on both nickel and Monel. These deposits were soft and sooty and were accompanied by graphitization within the metal.

The graphite specimens tested in this hydrogen—carbon monoxide atmosphere did not gain weight below 1350°F. Above 1350°F there was a measurable weight gain, with the maximum (2 mg/g, or 1 mg/cm^2 geometric area) occurring at 1600°F in 400 hr (see Fig. 40). This carbon deposit was very thin and was detectable only by the weight gain.

Exposure in 5×10^{-3} atm CO + 5×10^{-3} atm H_2

The exposures in 5×10^{-3} atm CO + 5×10^{-3} atm H_2 were conducted in a temperature gradient of 1700° to 150°F. There was no carbon deposited as free carbon in any of the experiments conducted at this impurity level. Table 8 summarizes the results of these exposures.

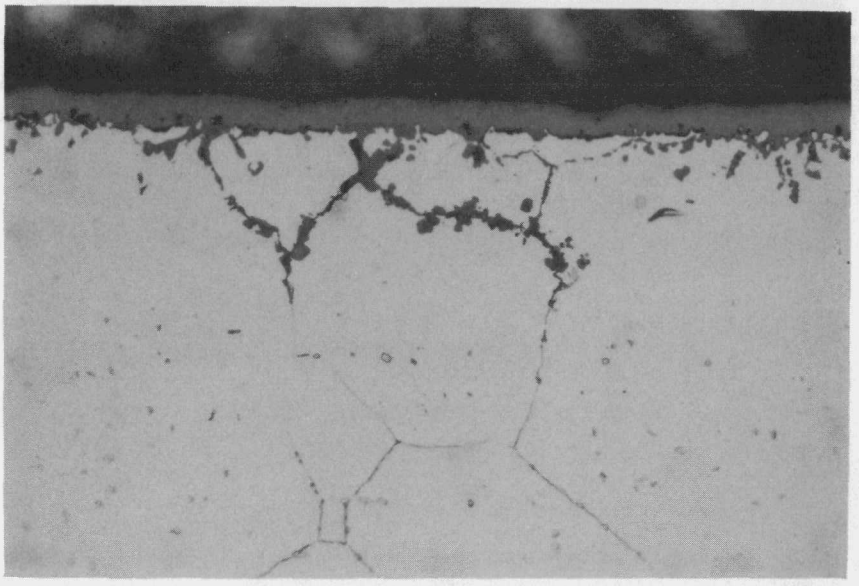

(a)

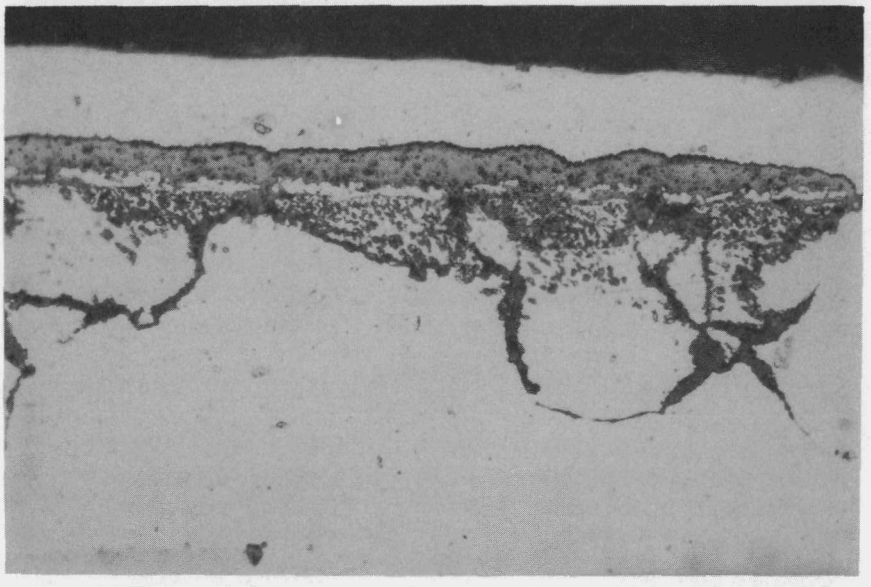

(b)

Fig. 39--Surface oxides formed on two types of Inconel after 400 hr at 1750°F in 0.5 atm CO + 0.5 atm H_2: (a) Inconel X; (b) Inconel 702 (500×)

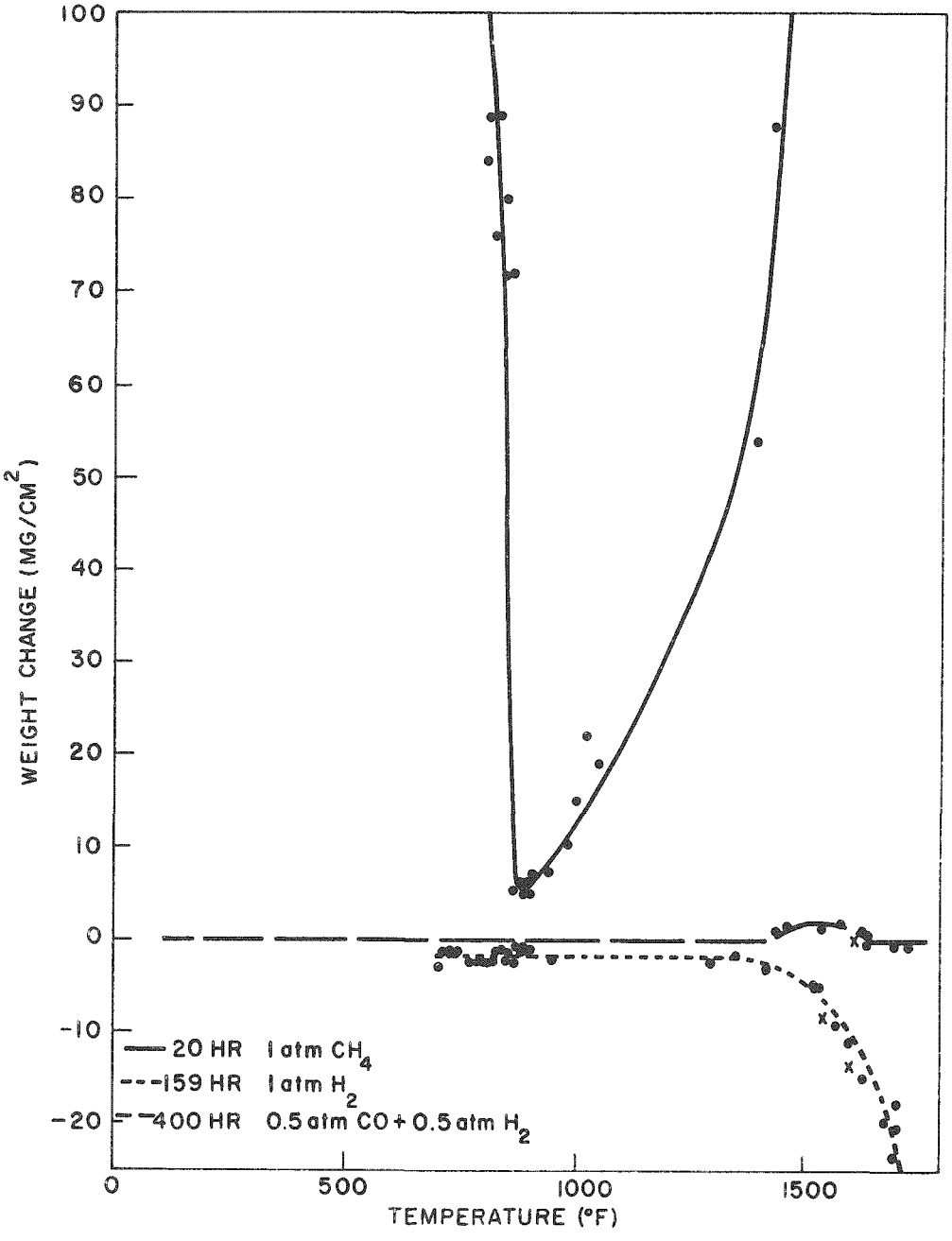

Fig. 40--Weight change versus temperature for AGOT graphite in various atmospheres

Table 8

SUMMARY OF RESULTS OF NICKEL- AND IRON-BASE ALLOYS EXPOSED TO 5×10^{-3} ATM CO + 5×10^{-3} ATM H_2

Material	Time (hr)	Temp. (°F)	Penetr. (mils)	Per cent Carbon		Corrosion Products*	Weight Change (mg/cm^2)	Remarks
				Initial	Final			
316 SS	1000	140	<0.1	0.05	-----	None	-0.03	
	1000	390	<0.1	0.05	0.056	None	-0.01	
	1000	730	<0.1	0.05	0.057	None	-0.005	
	1000	1150	0.1	0.05	0.096	None	0.13	
	1000	1440	10.0	0.05	1.09	$(Spinel)_w$	3.35	Carburized
	1000	1620	4.0	0.05	0.144	$(Spinel)_s$	0.92	Internal oxidation
	1000	1700	0.3	0.05	0.068	$(Spinel)_s$	0.26	
C–1/2 Mo	1000	150	<0.1	0.14	0.14	None	-0.0236	
	1000	200	<0.1	0.14	0.15	None	-0.0472	
	1000	480	<0.1	0.14	0.14	None	-0.118	
	1000	800	<0.1	0.14	0.15	None	-0.212	
	1000	950	<0.1	0.14	0.14	None	-0.118	
430 SS	1000	160	<0.1	0.080	0.082	None	-0.015	
	1000	440	<0.1	0.080	0.060	None	-0.01	
	1000	770	<0.1	0.080	0.055	None	-0.005	
	1000	1200	<0.1	0.080	0.070	None	0.000	
	1000	1480	<0.1	0.080	0.088	$(Spinel)_m$, $(Cr_2O_3)_w$	0.305	
	1000	1640	>30	0.080	0.73	$(Spinel)_s$, $(Cr_2O_3)_w$	4.56	Completely carburized
	1000	1700	>30	0.080	0.67	$(Spinel)_s$, $(Cr_2O_3)_m$	3.445	Completely carburized; 6.0-mil oxidation pits
1-1/4 Cr–1/2 Mo	1000	170	<0.1	0.10	0.108	None	-0.0147	
	1000	250	<0.1	0.10	0.08	None	0.000	
	1000	600	<0.1	0.10	0.10	None	-0.044	
	1000	890	<0.1	0.10	0.136	None	0.044	
	1000	1020	<0.1	0.10	0.20	None	0.0588	

*The subscript s is the small diffraction pattern; m, the medium diffraction pattern; and w, the weak diffraction pattern.

Table 8--continued

Material	Time (hr)	Temp. (°F)	Penetr. (mils)	Per cent Carbon		Corrosion Products*	Weight Change (mg/cm^2)	Remarks
				Initial	Final			
Inconel 702	1000	180	<0.1	0.030	0.031	None	-0.035	
	1000	520	<0.1	0.030	0.027	None	-0.035	
	1000	830	<0.1	0.030	0.031	None	-0.005	
	1000	1250	5.0	0.030	1.30	$[(Cr, Fe)_2O_3]_s$	8.265	Internal oxidation
	1000	1520	>30	0.030	0.60	$[(Cr, Fe)_2O_3]_s$	5.775	Completely carburized; 4.0-mil internal oxidation
	1000	1640	0.5	0.030	0.041	None	0.12	
	1000	1700	1.0	0.030	0.034	None	0.16	
Inconel X	1000	220	<0.1	0.035	0.036	None	-0.025	
	1000	560	<0.1	0.035	0.033	None	-0.02	
	1000	860	<0.1	0.035	0.042	None	-0.02	
	1000	1300	4.0	0.035	0.180	$[(Cr, Fe)_2O_3]_m$	0.99	Carburized; 1.0-mil surface oxide
	1000	1550	1.5	0.035	0.050	$[(Cr, Fe)_2O_3]_s$, $(spinel)_s$	0.69	Internal oxidation
	1000	1670	2.0	0.035	0.070	$[(Cr, Fe)_2O_3]_s$, $(spinel)_s$	1.68	Internal oxidation
	1000	1690	2.5	0.035	0.040	$[(Cr, Fe)_2O_3]_s$, $(spinel)_s$	1.69	Internal oxidation
Molybdenum	1000	100	<0.1	-----	-----	None	0.005	
	1000	130	<0.1	-----	-----	None	-0.010	
	1000	170	<0.1	-----	-----	None	0.000	
	1000	210	<0.1	-----	-----	None	-0.005	
	1000	260	<0.1	-----	-----	None	-0.005	
	1000	350	<0.1	-----	-----	None	0.000	
	1000	450	<0.1	-----	-----	None	-0.010	
	1000	550	<0.1	-----	-----	None	-0.010	
	1000	650	<0.1	-----	-----	None	-0.015	
	1000	740	<0.1	-----	-----	None	-0.015	
	1000	820	<0.1	-----	-----	None	-0.010	
	1000	900	<0.1	-----	-----	None	-0.010	

*The subscript s is the small diffraction pattern; m, the medium diffraction pattern; and w, the weak diffraction pattern.

Table 8--continued

Material	Time (hr)	Temp. (°F)	Penetr. (mils)	Per cent Carbon		Corrosion Products*	Weight Change (mg/cm^2)	Remarks
				Initial	Final			
Molybdenum--continued	1000	1000	<0.1	-----	-----	None	-0.010	
	1000	1120	<0.1	-----	-----	None	-0.005	
	1000	1240	<0.1	-----	-----	$(Mo_2C)_w$	0.015	Brittle
	1000	1350	0.1	-----	-----	$(Mo_2C)_s$	0.040	Brittle
	1000	1430	0.25	-----	-----	$(Mo_2C)_s$	0.115	Brittle
	1000	1500	0.40	-----	-----	$(Mo_2C)_s$	0.22	Brittle
	1000	1560	0.40	-----	-----	$(Mo_2C)_s$	0.29	Brittle
	1000	1610	0.60	-----	-----	$(Mo_2C)_s$	0.365	Brittle
	1000	1650	0.65	-----	-----	$(Mo_2C)_s$	0.41	Brittle
	1000	1700	0.65	-----	-----	$(Mo_2C)_s$	0.44	Brittle
	500	1700	0.50	-----	-----	$(Mo_2C)_s$	0.32	Brittle
	1000	1650	0.70	-----	-----	$(Mo_2C)_s$	0.45	Brittle
Nb-20 Ti	1000	420	<0.1	0.03	0.027	None	-0.01	480 ppm final oxygen content
	1000	630	<0.1	0.03	0.038	None	0.015	115 ppm final oxygen content
	1000	890	<0.1	0.03	0.024	None	0.11	650 ppm final oxygen content
	1000	1200	<0.1	0.03	0.026	$(Nb_2C)_w$	0.42	600 ppm final oxygen content
	1000	1380	0.5	0.03	0.067	$(TiC)_m$, $(Nb_2C)_w$, $(NbO_2)_w$	0.88	3,050 ppm final oxygen content; 1.0-mil cracks in brittle surface
	1000	1530	0.5	0.03	0.158	(Nb_2O_5)?$(TiC)_m$, $(Nb_2C)_w$, $(NbC)_s$	2.185	3,210 ppm final oxygen content; 2.0-mil cracks in brittle surface
	1000	1630	<0.1	0.03	0.27	(Nb_2O_5)?$(Nb_2C)_m$, $(NbC)_m$, $(TiC)_m$	3.99	5,590 ppm final oxygen content
	1000	1670	<0.1	0.03	0.24	None	5.17	8,640 ppm final oxygen content
Copper	500	1600	---	-----	-----	None	-0.11	Blistered
	500	1700	---	-----	-----	None	-0.135	Blistered
	500	1670	---	-----	-----	None	-0.17	Blistered
	500	1590	---	-----	-----	None	-0.12	Blistered
	500	1460	---	-----	-----	None	-0.115	Blistered
	500	1300	---	-----	-----	None	-0.12	
	500	1070	---	-----	-----	None	-0.03	
	500	760	---	-----	-----	None	-0.055	

*The subscript s is the small diffraction pattern; m, the medium diffraction pattern; and w, the weak diffraction pattern.

Table 8--continued

Material	Time (hr)	Temp. (°F)	Penetr. (mils)	Per cent Carbon		Corrosion Products*	Weight Change (mg/cm^2)	Remarks
				Initial	Final			
Nickel	1000	290	<0.1	0.030	-----	None	-0.04	
	1000	630	<0.1	0.030	0.035	None	0.01	
	1000	920	1.0	0.030	0.033	None	-0.01	Grain-boundary attack
	1000	1300	2.0	0.030	0.044	None	0.04	Grain-boundary attack
	1000	1580	1.0	0.030	0.012	None	-0.02	Grain-boundary attack
	1000	1600	1.0	0.030	0.04	None	0.015	Grain-boundary attack
	1000	1680	<0.1	0.030	0.013	None	0.52	Graphite precipitation in metal
	1000	1680	1.0	0.030	0.025	None	-0.01	Grain-boundary attack
Monel	1000	340	<0.1	0.096	-----	None	-0.015	
	1000	690	<0.1	0.096	0.069	None	0.015	
	1000	980	<0.1	0.096	0.070	None	-0.035	
	1000	1400	3.0	0.096	0.031	None	0.025	Grain-boundary attack
	1000	1600	11.0	0.096	0.018		-0.11	Grain-boundary attack
	1000	1680	15.0	0.096	0.022		-0.14	Grain-boundary attack
	1000	1650	3.0	0.096	0.026		0.135	Grain-boundary attack
Nb–1 Zr	500	1300	0.2	0.004	0.006	$(Nb_2C)_w$	0.115	
	500	760	<0.1	0.004	0.017	$(Nb_2C)_w$	0.02	
	500	1070	<0.1	0.004	0.013	$(Nb_2C)_w$	0.07	
	500	1460	<0.1	0.004	0.012	$(Nb_2C)_s$, $(NbC)_m$	0.13	
	500	1590	<0.1	0.004	0.066	$(Nb_2C)_s$, $(NbC)_s$	0.375	
	500	1670	<0.2	0.004	0.093	$(Nb_2C)_s$, $(NbC)_s$	0.645	
	500	1700	0.3	0.004	0.097	$(Nb_2C)_s$, $(NbC)_s$, $(NbO)_w$	0.83	
	500	1600	0.5	0.004	0.087	$(Nb_2C)_s$, $(NbC)_s$, $(NbO)_w$	2.39	

*The subscript s is the small diffraction pattern; m, the medium diffraction pattern; and w, the weak diffraction pattern.

Table 8--continued

Material	Time (hr)	Temp. (°F)	Penetr. (mils)	Per cent Carbon Initial	Per cent Carbon Final	Corrosion Products*	Weight Change (mg/cm^2)	Remarks
Niobium	1000	490	<0.1	<0.01	<0.01	None	-0.007	610 ppm final oxygen content
	1000	700	<0.1	<0.01	<0.01	None	0.033	580 ppm final oxygen content
	1000	980	<0.1	<0.01	0.017	None	0.073	470 ppm final oxygen content
	1000	1250	<0.1	<0.01	0.009	$(Nb_2C)_w$	0.133	685 ppm final oxygen content
	1000	1420	0.2	<0.01	0.021	$(Nb_2C)_w$, $(NbC)_s$	0.153	652 ppm final oxygen content
	1000	1560	0.7	<0.01	0.025	$(Nb_2C)_s$, $(NbC)_s$	0.400	113 ppm final oxygen content
	1000	1650	1.5	<0.01	0.033	$(Nb_2C)_s$, $(NbC)_s$	0.507	1,339 ppm final oxygen content
	1000	1700	0.5	<0.01	0.062	$(Nb_2C)_s$, $(NbC)_s$	0.890	800 ppm final oxygen content
	1000	1640	13	<0.01	0.72	$(NbO)_m$, $(NbO_2)_s$, $(NbC)_s$, $(Nb_2C)_s$	6.78	9,640 ppm final oxygen content
Nb-8 Ti	1000	350	<0.1	0.03	0.049	None	-0.025	540 ppm final oxygen content
	1000	560	<0.1	0.03	0.039	None	-0.005	485 ppm final oxygen content
	1000	820	<0.1	0.03	0.050	None	0.085	1,720 ppm final oxygen content
	1000	1150	<0.1	0.03	0.061	$(Nb_2C)_w$	0.16	732 ppm final oxygen content
	1000	1340	<0.1	0.03	0.080	$(NbC)_w$, $(Nb_2C)_w$	0.385	1,960 ppm final oxygen content
	1000	1500	<0.1	0.03	0.15	$(NbC)_m$, $(Nb_2C)_w$	0.715	4,940 ppm final oxygen content
	1000	1610	<0.1	0.03	0.29	$(NbO)_w$, $(NbO_2)_w$, $(NbC)_m$, $(Nb_2C)_m$	2.33	11,940 ppm final oxygen content
	1000	1690	<0.1	0.03	0.36	$(NbO)_w$, $(NbO_2)_w$, $(NbC)_m$, $(Nb_2C)_m$	3.19	9,640 ppm final oxygen content
	1000	1690	<0.1	0.03	0.32	$(NbO)_w$, $(NbO_2)_s$, $(NbC)_s$, $(Nb_2C)_s$	3.83	6,740 ppm final oxygen content
	1000	250	<0.1	0.03	0.049	None	-0.005	188 ppm final oxygen content

*The subscript s is the small diffraction pattern; m, the medium diffraction pattern; and w, the weak diffraction pattern.

The low-alloy steels exhibited low to moderate weight changes below 1000°F--no corrosion products were detected by X-ray diffraction measurements. The results indicate that these materials will perform satisfactorily at temperatures below 900°F at this impurity level.

At temperatures below 1480°F, Type 430 stainless steel did not carburize in this environment; however, above 1480°F it was completely carburized and was badly oxidized in 1000 hr. Large pits, 6.0 mils deep, filled with oxide were formed at 1700°F in 1000 hr. Type 316 stainless steel carburized at 1150°F and above. The carburization was particularly severe on the specimen exposed at 1440°F (see Fig. 41).

Inconel 702 formed a substantial surface layer of $(Cr, Fe)_2O_3$ at 1250°F and exhibited a large weight gain (8.3 mg/cm^2) in 1000 hr. The specimens exposed at 1250° and 1520°F were badly carburized and internally oxidized (see Fig. 42).

Inconel X was more resistant to attack by this environment than Inconel 702; i.e., the weight gains were smaller and the internal oxidation that occurred penetrated to a maximum depth of 2.5 mils. This alloy did, however, carburize in 1000 hr at 1300°F.

Molybdenum resisted attack at temperatures up to 1200°F; below this temperature there was no carbon deposition, no attack was observed metallographically, and there was no significant weight change. At 1240°F, Mo_2C (0.1 mil thick) was identified on the surface. This specimen was very brittle in a simple bend test, as were those tested at higher temperatures. The depth of penetration and accompanying weight gain increased with increasing temperature (see Fig. 43).

The niobium and niobium alloys showed weight gains in this atmosphere similar to those exhibited in 1 atm CO (Figs. 44 through 46). Chemical analysis revealed that some oxygen pickup occurred at the higher temperatures.

Nickel and Monel showed very small weight changes in this environment. Both materials, however, were attacked at the grain boundaries,

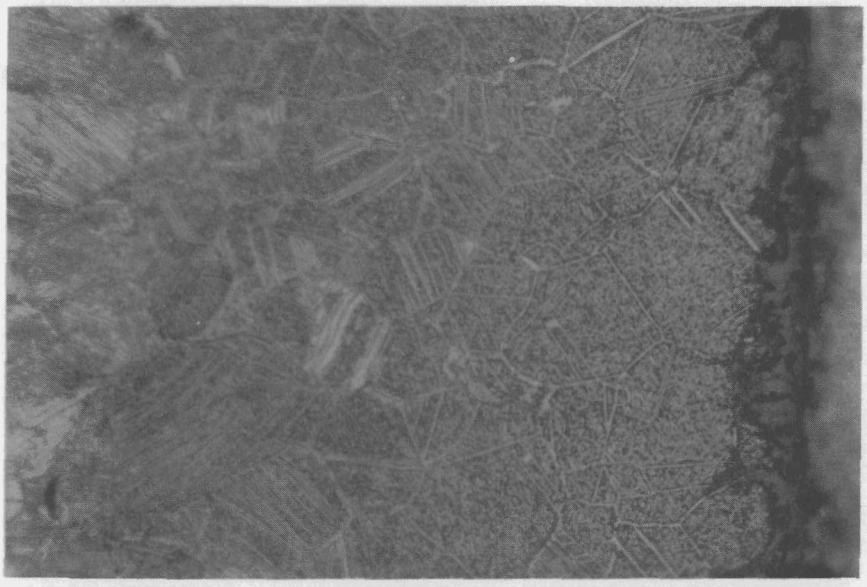

Fig. 41--Carburization on Type 316 stainless steel after 1000 hr at 1440°F in 5×10^{-3} atm CO + 5×10^{-3} atm H_2 (500×)

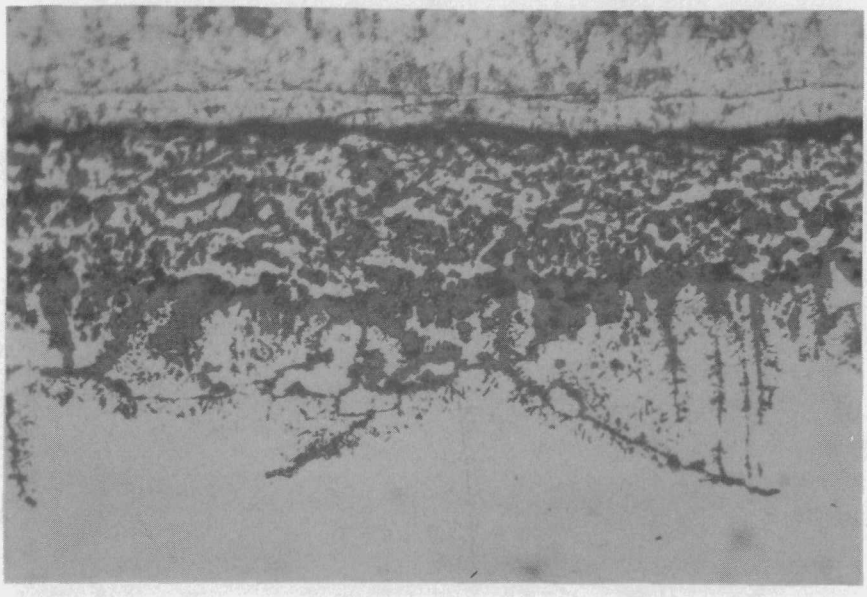

Fig. 42--Inconel 702 exposed for 1000 hr at 1520°F in 5×10^{-3} atm CO + 5×10^{-3} atm H_2--internal oxidation 6.0 mils deep (500×)

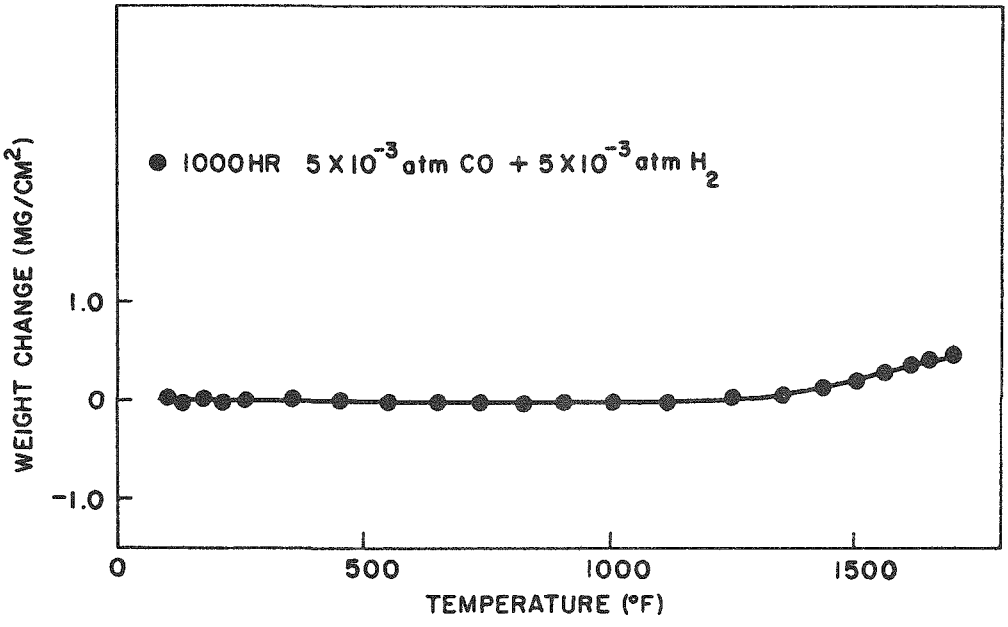

Fig. 43--Weight change versus temperature for molydenum specimens tested in helium with a low partial pressure of H_2 + CO

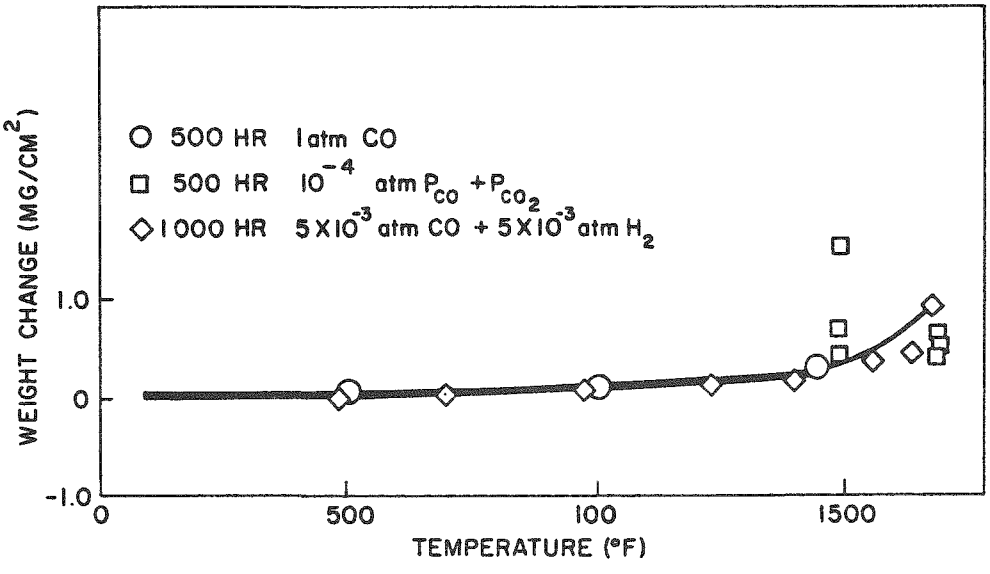

Fig. 44--Weight change versus temperature for niobium specimens tested in helium with various partial pressures of contaminants

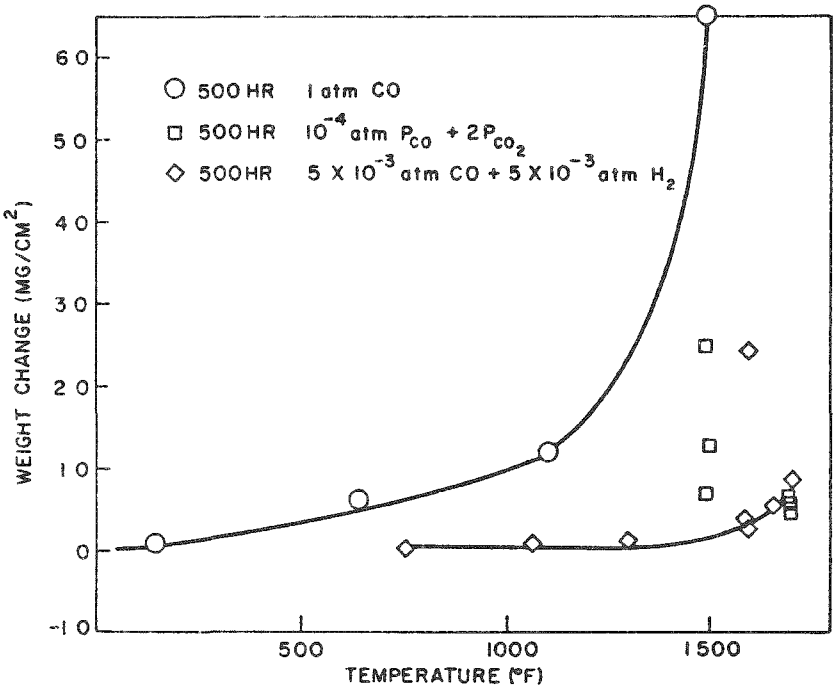

Fig. 45--Weight change versus temperature for niobium + 1% Zr specimens tested in helium at various partial pressures of contaminants

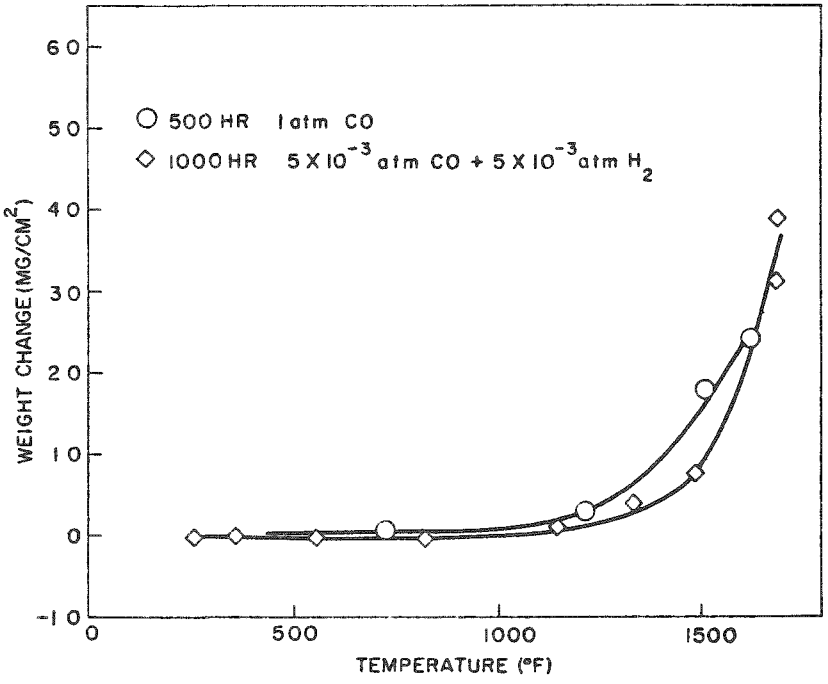

Fig. 46--Weight change versus temperature for niobium + 8% Ti specimens tested in helium at various partial pressures of contaminants

the attack being more severe on Monel at 1400°F and above (see Fig. 47). This grain-boundary attack was not observed in reducing atmospheres when Monel was embedded in graphite and it is probably observed here as a result of the alternate reducing and oxidizing conditions. Considerable water was detected at the outlet of the system during the course of the experiments conducted at this impurity level.

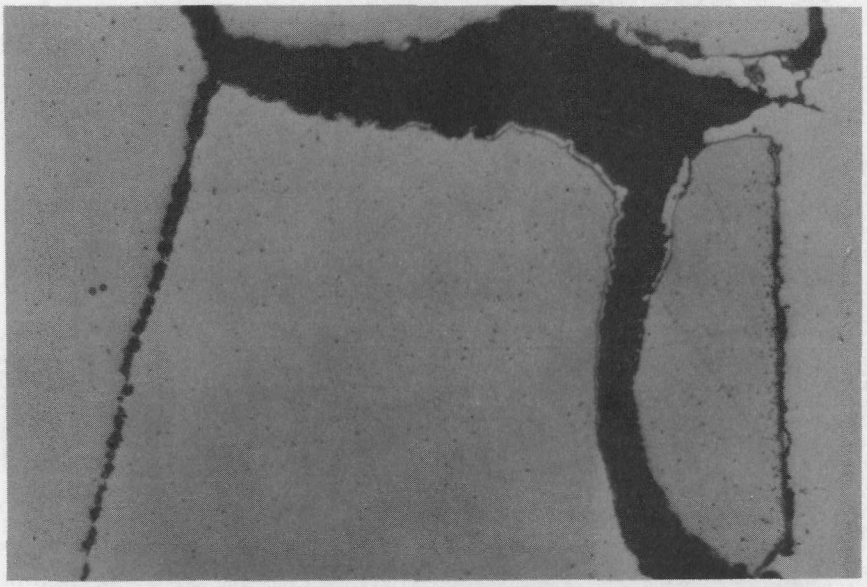

Fig. 47--Intergranular attack observed on Monel exposed for 1000 hr at 1600°F in 5×10^{-3} atm CO + 5×10^{-3} atm H_2

The behavior of copper in this environment was particularly interesting. Specimens exposed at 760°F developed voids at the grain boundaries in 500 hr (see Fig. 48a); at 1070°F, these voids completely outlined the grain boundaries (see Fig. 48b); above 1500°F, they agglomerated to form large central cavities, causing severe blistering. This behavior is believed to be the result of the internal reaction of hydrogen and oxygen to form water vapor.

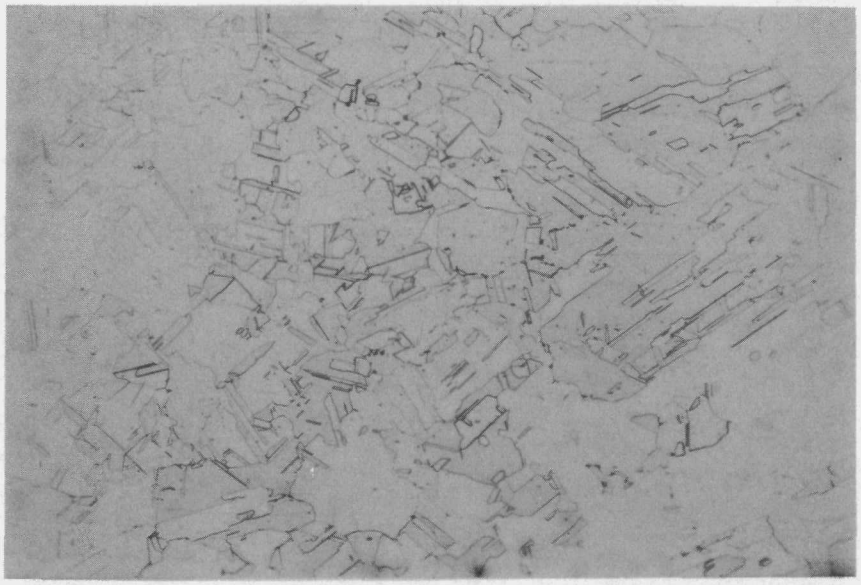

(a)

(b)

Fig. 48--Photomicrographs of copper exposed in 5×10^{-3} atm H_2 + 5×10^{-3} atm CO for 500 hr: (a) at 760°F a few voids are evident; (b) at 1070°F many voids have formed at grain boundaries (150×)

DISCUSSION AND CONCLUSIONS

From the observation of the previously described tests, it does not appear that niobium or any of the niobium-base alloys can be used in the unclad, graphite-moderated version of the MGCR. Although niobium does not catalyze the carbon monoxide disproportionation, its tolerance for oxygen is too low to be practical. The specimens tested in 2×10^{-4} atm ($P_{CO} + 2P_{CO_2}$) were embrittled in 100 hr. This was particularly true in the experiments conducted at 1500°F, where the graphite–CO-CO_2 equilibrium was not attained and a CO_2-rich gas reached the metal specimens. Since this level was significantly less than the partial pressure equivalent to 1 ppm of CO_2 in the MGCR, it seems unrealistic to assume that impurity levels lower than this could be maintained continuously in the reactor. The data on weight gain versus time for atmospheres that produce only carburization indicate that the carburization rate decreases with time; i. e., the carbide layer is protective for at least the period of time of the test.

Molybdenum did not catalyze carbon deposition in 5×10^{-3} atm CO + 5×10^{-3} atm H_2, and showed no measurable weight change below 1200°F. At 1200°F, molybdenum showed a very small weight gain due to the formation of a surface carbide. The formation of this carbide layer was accompanied by severe embrittlement. If this embrittlement can be eliminated, a molybdenum alloy would be an excellent high-strength material for use in the MGCR turbine.

Nickel and Monel were tested as possible candidates for cladding in the semihomogeneous fuel element.[9] Although these materials catalyze carbon monoxide disproportionation at high concentrations of carbon monoxide, they do not catalyze free-carbon deposition at levels of 10^{-2} atm CO or less. Under conditions anticipated for the MGCR, i. e., where Monel-clad fuel elements would be embedded in graphite, the tests indicated that there would be no carbon deposition or corrosion of the surface of either material. In the case of nickel, however, the temperature dependence of

carbon solubility causes graphitization during thermal cycling; i. e., at high temperature nickel becomes saturated with carbon, which precipitates when nickel is cooled. This "graphitization" can occur over a very narrow temperature range and will ultimately cause deterioration during thermal cycling. Monel has a lower solubility for carbon than nickel and does not graphitize significantly during thermal cycling. It did, however, suffer from extensive grain-boundary attack in the presence of mixtures of CO, CO_2, H_2, H_2O, and O_2. This type of attack was not observed when Monel was embedded in graphite (as it would be in the semihomogeneous fuel element) and exposed to impure high-pressure helium.[9] The presence of this grain-boundary attack in these tests may be attributed to alternate oxidizing and reducing conditions in gas mixtures.

Various high-strength nickel-base alloys were tested as potential turbine and structural materials. Inconel 702 was severely oxidized internally as well as carburized at temperatures above 1000°F. The weight gains in various atmospheres are plotted in Fig. 32. Inconel X was the most promising high-temperature, high-strength nickel-base alloy tested. It resisted severe carburization and oxidation better than the other high-strength nickel-base alloys tested and was ineffective in catalyzing the carbon monoxide disproportionation at impurity levels expected in the MGCR system. Further long-term physical tests will be necessary to determine the long-term effects of carburization and corrosion on strength.

The weight gains for Type 316 stainless steel in various atmospheres are plotted in Fig. 35. These tests indicate that this stainless steel would be satisfactory for use in the MGCR only below 1100°F.

Type 430 stainless steel was tested because it is a typical ferritic stainless steel. The weight gains in various atmospheres are plotted in Fig. 34. These tests indicate that Type 430 stainless steel could be used at temperatures of 1300°F or less with no significant carburization if the CO-H_2 partial pressure were maintained below approximately 10^{-2} atm

in the reactor system. This steel was the most carburization-resistant steel tested and was superior to all others in its failure to catalyze carbon monoxide disproportionation.

The low-alloy steels tested carburize badly in atmospheres containing a high partial pressure of carbon monoxide at temperatures above approximately 1000°F. For the MGCR system, these steels could be used as piping materials up to about 900°F.

The weight-gain data from tests conducted with graphite in hydrogen, methane, and 0.5 atm H_2 + 0.5 atm CO are plotted in Fig. 41. The results indicate that very little methane is formed below 1300°F by the reaction of carbon with hydrogen. The methane will decompose on most materials and certainly on carbon if the methane is in a region of thermodynamic instability. The H_2 + CO reactions do not deposit measurable carbon on graphite below 1350°F. Since 1300°F is the tentative exhaust gas temperature for the MGCR, it seems very unlikely that the transport of carbon across the reactor due to thermal reactions would be a serious problem if hydrogen levels were maintained reasonably low ($\sim 10^{-2}$ atm).

Calculations by Thompson,[10] based on Ragone's analysis, set the CO + $2CO_2$ level at a maximum of 10 ppm for tolerable carbon transport. This calculation was made assuming that the rate-limiting process is the diffusion of carbon monoxide from the gas stream to a metallic surface where the carbon monoxide to carbon dioxide disproportionation would be catalyzed. This calculated limit is in good agreement with experimental observations; however, for the short periods of the tests (up to 1000 hr), carbon was deposited from the gas mixtures containing $<10^{-2}$ atm impurity by reacting with the metal to form carbides. The experimental results point out some metals which do not act as active catalysts at any temperature, such as molybdenum and niobium alloys. Other metals are ineffective catalysts in specific temperature ranges. Proper selection of materials could reduce the carbon mass transport to below the amount calculated from Ragone's analysis. Other metals such as low-alloy steels are

destructively carburized, so that the permissible impurity level for these metals must be based on the tolerable carburization of the material and not on the gross carbon mass transport.

REFERENCES

1. Pigford, T. H., Gas-cooled Reactor Plants for Marine Propulsion, General Atomic Report GA-479, August 21, 1958.
2. Ragone, D. V., Kinetic Limitations to Carbon Deposition, General Atomic Report GAMD-960, September 3, 1959.
3. Baukloh, W., and G. Henke, Metallwirtschaft, Vol. 19, 1940, p. 463.
4. Baukloh, W., B. Chatterjee, and P. P. Das, Trans. Ind. Inst. Metals, Vol. 4, 1910, p. 271.
5. Das, P. P., and B. Chatterjee, Trans. Ind. Inst. Metals, Vol. 7, 1955, p. 189.
6. Chatterjee, B., and P. P. Das, "Nature of the Catalyst in the Decomposition of Carbon Monoxide in Presence of Iron," Nature, Vol. 173, 1954, p. 1046.
7. Horiba, S., and T. Ri, "Taylor's Theory of Active Centers and the Kinetics of Heterogeneous Gaseous Reactors," Rec. trav. chim., Vol. 51, 1932, p. 641.
8. Baukloh, W., and G. Hiber, Z. anorg. u. allgem. Chem., Vol. 226, 1936, p. 321.
9. Bokros, J. C., An Evaluation of Nickel-Copper Alloys for use as Graphite-cladding Material at Elevated Temperatures, General Atomic Report GA-1281, April 30, 1960.
10. Thompson, W. I., personal communication.